CLIMFILL v0.9: A Framework for Intelligently Gap filling Earth Observations

Verena Bessenbacher[1], Sonia I. Seneviratne[1], and Lukas Gudmundsson[1]

[1]ETH Zürich, Rämistrasse 101, 8092 Zürich, Switzerland

Correspondence: Verena Bessenbacher (verena.bessenbacher@env.ethz.ch)

Abstract. Remotely-sensed Earth observations have many missing values. The abundance and often complex patterns of these missing values can be a barrier for combining different observational datasets and may cause biased estimates of derived statistics. To overcome this, missing values in geoscientific data are regularly infilled with estimates through univariate gap filling techniques such as spatial or temporal interpolation, or by up-scaling approaches in which complete donor variables are used to infer missing values. However, these approaches do typically not account for information that may be present in other observed variables that also have missing values. Here we propose CLIMFILL (CLIMate data gap-FILL), a multivariate gap filling procedure that combines kriging interpolation with a statistical gap filling method designed to account for the dependence across multiple gappy variables. In a first stage an initial gap-fill is constructed for each variable separately using state-of-the-art spatial interpolation. Subsequently, the initial gap-fill for each variable is updated to recover the dependence across variables using an iterative procedure. Estimates for missing values are thus informed by knowledge of neighboring observations, temporal processes and dependent observations of other relevant variables. CLIMFILL is tested using gap-free ERA-5 reanalysis data of ground temperature, surface layer soil moisture, precipitation and terrestrial water storage to represent central interactions between soil moisture and climate. These variables were matched with corresponding remote sensing observations and masked where the observations have missing values. In this "perfect dataset approach" CLIMFILL can be evaluated against the original, usually not observed part of the data. We show that CLIMFILL successfully recovers the dependence structure among the variables across all land cover types and altitudes, thereby enabling subsequent mechanistic interpretations in the gap-filled dataset. Correlation between original ERA-5 data and gap filled ERA-5 data is high in many regions, albeit showing artefacts of the interpolation procedure in large gaps in high latitude regions during winter. Bias and noise in gappy satellite-observable data is reduced in most regions. A case study of the European 2003 heat wave shows how CLIMFILL reduces biases in ground temperature and surface layer soil moisture induced by the missing values. Furthermore, in idealised experiments we see the impact of fraction of missing values and the complexity of missing value patterns to the performance of CLIMFILL, showing that CLIMFILL for most variables operates at the upper limit of what is possible given the high fraction of missing values and the complexity missingness patterns. Thus, the framework can be a tool for gap filling a large range of remote sensing and in situ observations commonly used in climate and environmental research.

1 Introduction

1.1 Missing observations in Earth system science

Observing the Earth surface from space is an endeavour that has significantly contributed to advance our understanding of the Earth system and has played a vital role in the fields of data assimilation (Bauer et al., 2015), Earth surface modeling (Balsamo et al., 2018), global freshwater hydrology (Lettenmaier et al., 2015), global carbon cycle processes (Humphrey et al., 2018) and the study of climate extremes in the land-atmosphere system (Dorigo et al., 2017; Nicolai-Shaw et al., 2017; Teuling et al., 2010). A plethora of instruments observes variables relevant for determining the state of the Earth remotely at any given time. However, this observational record is highly fragmented: Remote sensing observations have a extensive spatial coverage, but differ in their spatial and temporal resolution, their frequency and temporal extent or suffer from inhomogeneities and measurement limitations (Lettenmaier et al., 2015; Shen et al., 2015; Seneviratne et al., 2010; de Jeu et al., 2008).

Moreover, the observational record suffers from complex, large-scale and unavoidable missing values that differ among variables. These missing values can hinder further analysis and can obscure physical dependencies between observations. Therefore, gap filling is common in the Earth system sciences. It is used to fill gaps originating from sensor failure or sensor limitations (Pastorello et al., 2020; Liu et al., 2018; Shen and Zhang, 2009), to extrapolate into under-sampled regions (Ghiggi et al., 2019; Gudmundsson and Seneviratne, 2015; Cowtan and Way, 2014; Jung et al., 2011, 2009) or to get estimates for regions obscured to the sensor by clouds, dense vegetation, flight geometry or other influences (Huffmann et al., 2019; Zeng et al., 2015; Brooks et al., 2012; Shen and Zhang, 2009).

In the geoscientific literature, among the most commonly used approaches for estimating unobserved points are spatial and temporal interpolation methods, including nearest neighbour regression as well as kriging and derivatives thereof (Liu et al. 2018; Cowtan and Way 2014; Haylock et al. 2008; Cressie et al. 2006, for an overview see Cressie and Wikle 2015; Chiles and Delfiner 2012). Spectral methods are used as well (Zhang et al., 2018; von Buttlar et al., 2014; Brooks et al., 2012). Shen et al. (2015) gives an overview over univariate spatial, temporal, spatiotemporal and spectral methods often used for gap filling remote sensing observations. In recent years, machine learning based approaches have become more common to fill gaps in univariate, gappy satellite data or up-scale sparse station networks (Kadow et al., 2020; Gerber et al., 2018; Zeng et al., 2015; Shen and Zhang, 2009). These methods are by default univariate, but can be extended into multivariate settings (Bhattacharjee and Chen, 2020; von Buttlar et al., 2014).

In the multivariate context, several data products exist that gap fill one or more observations to a spatially or temporally complete data sets using auxiliary variables (Huffmann et al., 2019; Brocca et al., 2014) or estimate variables that are only observed through sparse station networks via statistical up-scaling (O. and Orth, 2021; Zhang et al., 2021; Ghiggi et al., 2019; Jung et al., 2019; Martens et al., 2017; Gudmundsson and Seneviratne, 2015; Jung et al., 2011, 2009). Those approaches rely on gap-free "donor" dataset to infer values of incomplete variables, i.e. only one of the variables in the multivariate setting is

allowed to have missing values. In multivariate cases where more than one variable has missing values ad-hoc gap-fills are usually applied in the preprocessing (Pastorello et al., 2020; Jung et al., 2019; Martens et al., 2017; Tramontana et al., 2016). To our knowledge only a few notable exceptions (e.g. Mariethoz et al. 2012) to the common practice to focus on single gappy variables exist in the geoscientific literature.

In summary, geoscientific approaches often center around exploiting the spatial, temporal or spectral neighborhood of gaps to infer missing values. Furthermore, available methods are mostly focusing on estimating missing values in one single variable and can typically not be applied in a multivariate settings where missing values are observed in all considered datasets and a coherent, gap-free multivariate dataset is the aim. This implies that gap filling estimates of different variables may not be physically consistent and that available information may not be used efficiently if there are observations from more than one variable with missing values.

Nevertheless, combining observations from several, possibly gappy variables into a coherent "view" of the state of the Earth system is crucial for many applications. These include, but are not limited to, the analysis of local and regional land surface dynamics (Humphrey et al., 2018; Vogel et al., 2017), tracing of compound extreme events (Ridder et al., 2020; Wehrli et al., 2019) or observational water and energy budget closures (Alemohammad et al., 2017; Martens et al., 2017). The necessity of creating a global, physically coherent observational dataset of the Earth's state is also highlighted through international initiatives such as the Digital Twin Earth Initiative from ESA (Bauer et al., 2021b).

Atmospheric reanalyses can be viewed as another class of gap-free reconstructions of the state of the Earth system. They typically assimilate a wide range of observations into global weather models and are often the default dataset for a range of applications (Hersbach et al., 2020; Gelaro et al., 2017; Dee et al., 2011). However, since reanalysis products are by construction model-driven, they are subject to model biases (Bocquet et al., 2019) and issues with model independence can arise if reanalysis products are used for model validation. Moreover, the observational record of the Earths' surface is generally underutilised in state-of-the-art reanalysis products and the large fraction of missing values is on of the major constraints (Dorigo et al., 2017). For example, in the state-of-the-art atmospheric reanalysis product ERA-5 the fragmented observational record of soil moisture is used only sparsely (Hersbach et al., 2020), although the added value of assimilating remote sensing soil moisture has been shown for weather forecast models (Zhan et al., 2016) and flood forecasting (Brocca et al., 2014; Sahoo et al., 2013).

Given the current status of research in this field, Balsamo et al. (2018) note the need for more multivariate Earth observation datasets apart from reanalysis. At the same time, Bauer et al. (2021b) mention an ongoing trend to reshape classical reanalysis such that physical modeling and fragmented observation can be harmonised into a combined product by the use of machine learning techniques wherever processes are unknown or difficult to parameterise. In the following, we present an approach to consolidate fragmented Earth observations into a coherent, multivariate, gap-free dataset by tackling the problem of missing values in multivariate remotely-sensed Earth observations. Distinguishing the approach from reanalysis, we do not aim to
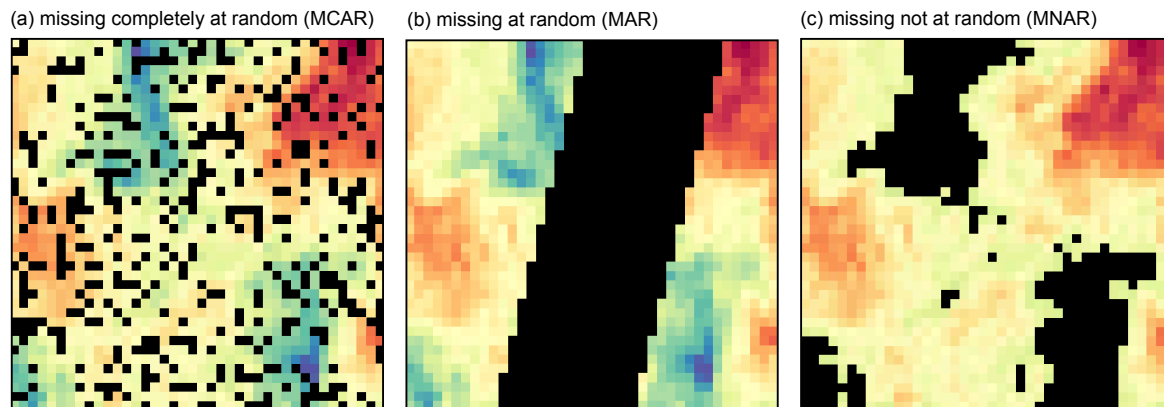
Figure 1. Examples of the three patterns in which values can be missing: (a) Missing completely at random (MCAR), (b) Missing at random (MAR) and (c) Missing not at random (MNAR). The MCAR missingness is created by setting randomly drawn grid points to be missing. For MAR missingness, a patch of the data was removed to mimic satellite swaths. In MNAR missingness, all values below a certain threshold are missing.

assimilate observations with a pre-defined physical model, but to leverage the power of modern statistical techniques to produce
95 dependable and physically consistent estimates of essential Earth system observations. The newly developed methodology is tested for variables relevant for the study of land-atmosphere dynamics.

1.2 Statistical concepts for treating missing values

The methodological literature offers a overarching framework for the problem of missing values (Rubin, 1976): Typically, the simplest form of gap management is referred to as list-wise deletion, where only data points are considered if all variables
100 are observed. However, this approach can lead to large data loss. Furthermore, statistics derived from incomplete data can be biased if the data are missing not at random (Rubin, 1976). Consequently, the pattern in which the data are missing (i.e., the "missingness") is one of the most important factors when estimating the impact of missing values (Little and Rubin, 2014). In particular, Rubin (1976) categorizes three ways in which data can be missing: missing completely at random (MCAR), missing at random (MAR) and missing not at random (MNAR). In the following these categories of missingness are described in the
105 context of Earth observations.

- If the probability that a data point is missing is not dependent of any process, the missingness is described as missing completely at random (MCAR, Figure 1 a). In the context of Earth observations this might be caused by random sensor failure, but it is rarely the dominant pattern of missingness.

- Satellite data are often missing because of satellite swaths. For example orbiting satellites, e.g. measuring soil moisture
110 with a microwave sensor, do not pass certain regions at certain times (Figure 1 b). Here, the fact that we can't measure

the soil moisture at a certain space-time point is not dependent on the actual soil moisture at this point. In other words, the soil moisture is not significantly lower or higher in the locations where the satellite does not pass through. Therefore, the probability of a data point missing is not dependent on the value of the missing data point. Such patterns are referred to as missing at random (MAR).

115 – The most complex missingness pattern is missing not at random (MNAR). Here, the mechanism that obscures data points depends on the data that are missing. This mechanism can be a function of the observed variables, for example when values above or below a certain threshold are not observable (Figure 1 c). Moreover, missingness might be controlled by a different, but related variable. In the case of a satellite measuring soil moisture via microwave retrievals, the measurement over dense vegetation represents the water content of the canopy rather than the one of the soil. Hence the data at such

120 points are masked during post-processing, leading to large patches of missing values especially in tropical forests. Here, we cannot safely assume that soil moisture below dense vegetation is not significantly different from observed soil moisture. Therefore, we cannot assume independence between the fact that a point is missing and the unobserved value of the missing point.

Geoscientific data are in a large part missing not at random (MNAR), making statistical measures of the data biased (van

125 Buuren, 2018; Rubin, 1976) and gap filling challenging (see for example Cowtan and Way 2014). Ghahramani and Jordan (1994) show that statistically motivated gap filling of missing data is possible for MCAR and MAR cases in both a Bayesian and a Maximum Likelihood setting, but note that MNAR data cannot be tackled with the same methods. However, gap filling can still be successful if a high degree of dependence between MNAR variables increases their mutual information. We argue that this is especially the case for geoscientific observations, since the variables are often directly linked through a number of

130 processes.

In statistical literature, a wide range of algorithms exist that make use of cross-variable dependence to estimate missing values. These center around low-rank matrix recovery, eigenvalue analysis or regression for estimating missing values (Davenport and Romberg, 2016; Mazumder et al., 2010). Here, in contrast to common geoscientific approaches, missing values in

135 all variables are allowed. In the following, we are highlighting two common approaches. On one hand, Gaussian processes are a natural choice for gap filling problems (Gelfand and Schliep, 2016) and are mathematically identical to kriging, if the predictors are latitude and longitude. Gaussian processes however have limitations when moving to large data (Heaton et al., 2019) as is the case in Earth observation data. In recent years, some applications of Gaussian processes have been shown to work in settings with too much data to estimate the co-variance matrix between all datapoints precisely. They estimate the

140 co-variance matrix via sophisticated sampling techniques (Wang and Chaib-draa, 2017; Das et al., 2018), pre-process the data via dimension reduction methods (Banerjee et al., 2008) or apply the Gaussian Process to local subsets of the data (Gramacy and Apley, 2015; Datta et al., 2016). On the other hand, iterative procedures like the MICE-Algorithm ("Multiple imputation by chained equation", van Buuren (2018)) are well suited for multivariate imputation and scale to large data, but cannot account for neighborhood relations. Regression-based multivariate gap filling algorithms like MICE have, to the best of our knowledge,

145 not yet been applied in the geoscientific context.

In the following Section 2), we propose the multivariate gap filling framework CLIMFILL that aims at overcoming the mentioned issues, combines the two approaches highlighted above and thus takes advantage of univariate interpolation techniques (Cressie et al., 2006) as well as approaches for improving cross-variable coherence (Stekhoven and Bühlmann, 2012).
150 In Section 3 we describe the data that has been used to evaluate the skill of the framework and in Section 4 we show the results of evaluating and benchmarking the framework. Finally, Sect. 5 discusses the results and provides a conclusion and an outlook for possible future work.

2 CLIMFILL v0.9: A Framework for Infilling Missing Values in Multivariate Spatio-Temporal Geoscientific Data

We aim to develop a multivariate gap filling framework that exploits the spatial, temporal and cross-variable dependence struc-
155 ture of Earth system observations to produce estimates for missing values even if they are present in all variables. To achieve this goal we build upon geo-statistical interpolation and a multivariate gap-filling approach that has been popularized in other fields, namely the MissForest algorithm (van Buuren, 2018; Stekhoven and Bühlmann, 2012). In particular, we aim at utilizing (1) spatial neighborhood information, (2) temporal correlation and (3) and statistical dependence across all considered variables. With these design requirements we aim at recovering both the marginal distributions and the dependence among
160 variables at any location with missing values. The CLIMFILL framework works mutually for all considered variables, i.e. information available in each of the variables is used for filling the gaps of all the other variables. With this design we implicitly assume that if one variable is not observed at a certain space-time point, a subset of the other variables might be observed and can reconstruct the missing value while conserving the dependence structure among all variables.

165 The framework is divided in four steps (Fig. 2): In a first step, initial estimates for all missing values are produced by spatial interpolation of each variable independently, i.e. in a univariate setting. In a second step, the data are pre-processed to account for spatial and temporal dependence, which contributes to approximate physical links among different variables. In the third step, the data are divided into environmentally similar clusters. In the forth and final step the multivariate dependencies are taken into account: the initial estimates from the interpolation step are updated by an iterative procedure that aims to reconstruct
170 the dependence structure between the variables with the aim of increasing the accuracy of the initial estimates.

2.1 Step 1: Interpolation for integrating spatial context

The interpolation step creates initial estimates based on the spatial or spatiotemporal context of the gap using interpolation. Following the approach of Haylock et al. (2008), the data is first divided into monthly climatology maps and anomalies. The climatology maps are gap filled using thin-plate-spline interpolation to represent the spatial trends in the data. Subsequently,
175 the daily anomalies from the monthly climatology are gap filled using kriging. In contrast to the E-OBS dataset created in Haylock et al. (2008) from in-situ observations, satellite data has a much larger number of observed values, making a direct
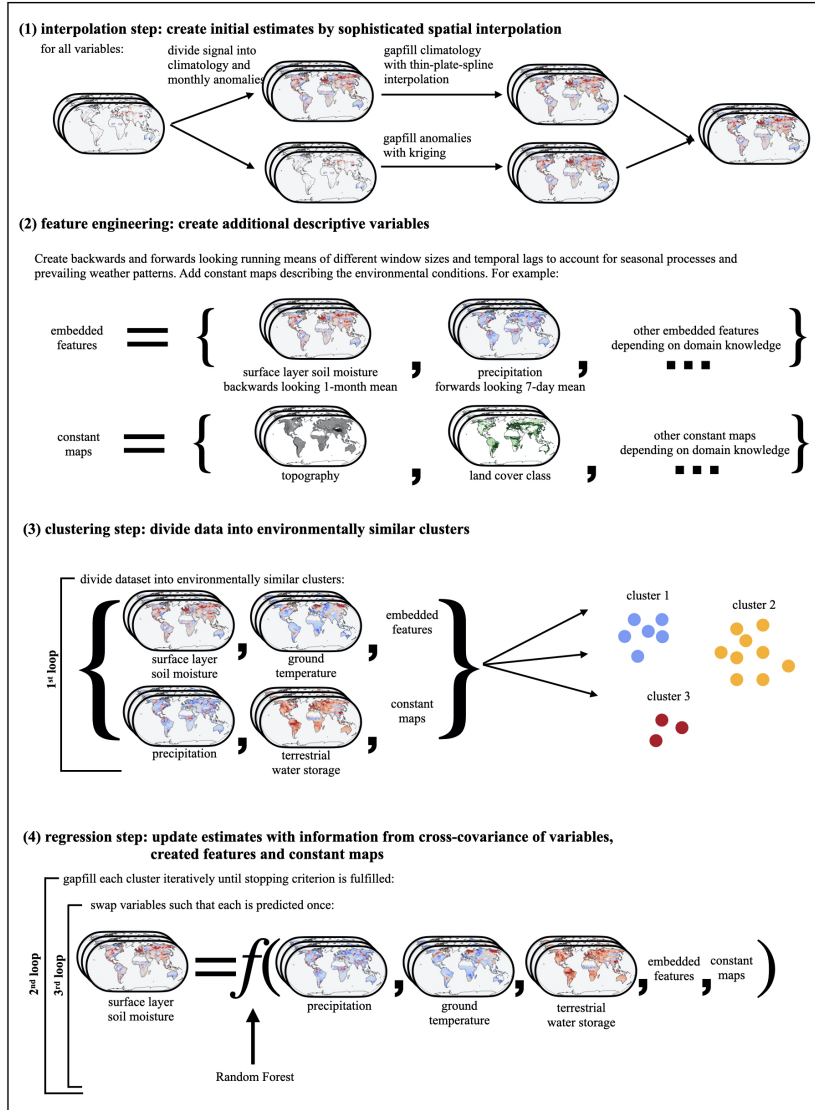
Figure 2. Overview on the structure of the gap filling framework. The framework is divided into four steps. In the first step (Sect. 2.1), any missing value is gap filled by an initial estimate from the spatio-temporal context. This step is called interpolation step. Here the spatio-temporal mean of observed values surrounding the missing value is used for each variable individually. In the second step (Sect. 2.2), embedded features are created to inform about time-dependent processes. In the third step, the data are divided into environmentally similar clusters (Sect. 2.3, Algorithm 1). In the forth step (Sect. 2.4, Algorithm 1), the inital estimates from step 1 are updated while accounting for the dependence structure among all considered variables. This is achieved by first grouping available data point into environmentally similar clusters and then iteratively updating the initial estimates using a supervised learning algorithm.
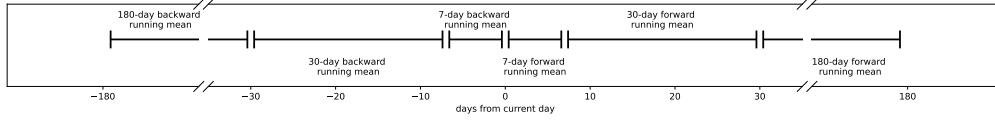
Figure 3. Time lags and window sizes of embedded features used in this study.

implementation of this approach computationally infeasible. For the interpolation of the monthly climatology maps we therefore restrict the thin-plate-spline interpolation to the 50 closest neighbors of each point. The interpolation of the daily anomalies follows Das et al. (2018), who suggest reducing complexity of kriging/Gaussian Process regression by repeated interpolations on random sub-samples of all available data points and averaging the resulting estimates. In particular, the missing values in the anomalies are estimated by randomly selecting 1000 observed points per month over which the interpolation is calculated. This is repeated five times and the mean of all interpolations for each missing point is taken as the gap-fill estimate. As a consequence of these adaptations, the interpolation step becomes computationally feasible, but the uncertainty of the interpolation cannot be estimated. Finally, monthly maps and anomalies are summed up to form the inital gap-fill estimate from step 1.

2.2 Step 2: Feature engineering informed by process knowledge

An important step in data driven modelling is taking care that the data consist of informative variables that represent the mechanisms at work. This creation of variables or "features" guided by expert knowledge is called feature engineering. Earth observations often inform about time dependent processes like seasonal effects, weather persistence or soil moisture memory effects that act from daily to monthly or subseasonal time scales (Nicolai-Shaw et al., 2016). To account for such antecedent and subsequent effects, backwards and forwards looking running means of different window size and temporal lags are included. This is motivated by prior work on large-scale runoff estimation (Gudmundsson and Seneviratne, 2015). Given a variable $v_{i,j,t}$ at longitude i, latitude j and time step t we define the window size s and time lag l over which a running mean of a variable v is computed:

$$v *_{i,j,t} (l,s) = \frac{1}{s} \left(v_{x,y,t-s-l} + v_{x,y,t-(s-1)-l} + ... v_{x,y,t-l} \right)$$ (1)

resulting in an embedded feature v^* produced from variable v. We create embedded features of 7-day ($s = 7, l = 0$), 1-month ($s = 23, l = 7$) and 6-month ($s = 150, l = 30$) backward and forward running means in such way that the windows are not overlapping (see Fig. 3). This way six additional features are created for each variable. Furthermore, gap-free time-independent maps describing properties of the land surface such as topography or land cover can be included. Maps of altitude, topographic complexity, land cover class and land cover height from ERA-5 as well as latitude, longitude and time are added to the list of features and copied for each time step.

The above procedure thus results in a set of 34 features: The four variables, the six embedded features of each of the four variables, totalling in 24 embedded features, the six maps and latitude, longitude and time information. All data are standardized to have zero mean and a standard deviation of one. We perform feature selection experiments (see Section 2.2) to find the most descriptive subset of these 34 features, which we then use for computing the results.

2.3 Step 3: Grouping the data into environmentally similar clusters

Depending on the climate regime and the season, different processes might govern the local dependence among variables. Furthermore, geoscientific datasets are very large and the computational costs of supervised learning methods does often not scale linearly with the number of samples. We therefore split the data into K environmentally similar clusters $\mathbf{X}^{(1)}, ..., \mathbf{X}^{(K)}$ (Algorithm 1, line 3) in which the multivariate gap filling happens (Algorithm 1, first loop, line 4+16). This grouping is done in such way that grid points can be in different clusters at different time steps. For example, a grid point in the Mediterranean area can be in a different cluster in winter than in summer, accounting for seasonally varying climate phenomena such as changing soil moisture regimes (Seneviratne et al., 2010). Here a K-means algorithm is used and the data are partitioned into 30 clusters. This value is chosen such that the number of data points per cluster is sufficiently large to ensure that the regression model can be calibrated efficiently, but not too small such that no individual clusters consist of missing values entirely.

2.4 Step 4: Optimising the initial estimates by accounting for the dependence between variables

In the fourth step, the initial estimates from step 1 are updated by accounting for the dependence between variables. Within each of the clusters $\mathbf{X}^k$, the algorithm repeatedly iterates over the variables until convergence is reached. This procedure builds upon the MissForest algorithm by Stekhoven and Bühlmann (2012). For each variable v, a Random Forest model (Breiman, 2001) is fitted to the cluster to predict originally missing values in all variables based on the remaining features. Random Forests have have favorable properties for gap filling applications: they can handle mixed types of data, are scalable to large amounts of data and non-parametric, i.e. adaptive to linear and non-linear relationships (Tang and Ishwaran, 2017).

This core mechanism of CLIMFILL is detailed in the inner, third loop of Algorithm 1 (line 6 to 14): The current variable is selected from the cluster as predictand $\mathbf{y}_v^k$. All other columns of $\mathbf{X}^k$ form the predictor table $\mathbf{X}_{-v}^k$, where $-v$ denotes the set of all variables and features except v. Subsequently both $\mathbf{y}_v^k$ and $\mathbf{X}_{-v}^k$ are divided into two sets of data points: (1) all data points where $\mathbf{y}_v^k$ was originally observed are used to fit the supervised learning method $\mathbf{y}_{v,o}^k = f(\mathbf{X}_{-v,o}^k)$ and (2) all data points where $\mathbf{y}_v^k$ was missing $\mathbf{y}_{v,m}^k$ are predicted from the fitted function to overwrite the former estimates: $\hat{\mathbf{y}}_{v,m}^k = f(\mathbf{X}_{-v,m}^k)$. Note that the training data most likely include originally missing values in the predictor variables. Here, the estimates from the interpolation step play the role of giving an initial estimate in the first iteration. Once the algorithm has iterated over all the variables, each missing value has been updated once. The algorithm is stopped (stopping criterion, Algorithm 1, second loop, line 5+15) once the change in the estimates for the missing values is small between iterations (convergence) or a maximum number of iterations

235 is reached (early stopping).

Note that the framework is set up such that each cluster learns different model parameters. With these choices the model is flexible to tailor its hyper-parameters individually to each variable and the regression parameters individually to each cluster. The hyper-parameters of the interpolation and the regression step are largely determined by computational limits of the

240 available resources (for an overview see Table A2). Where possible, we calibrated the remaining hyper-parameters by cutting out spatiotemporal cubes of observed data in year 2013 and compare values gap filled with CLIMFILL with the originally observed ones.

Algorithm 1 Pseudo-code algorithm of the CLIMFILL clustering and learning step (step 3 and 4), where K is the number of clusters, n_v is the number of variables and n_f the number of features. $\mathbf{X}_{-v}$ refers to the data table with all variables (columns) except v. Algorithm and pseudo-code are adapted from Stekhoven and Bühlmann (2012).

1: $\mathbf{X}$ is a matrix containing all variables and features as $n_v + n_f$ columns and all data points as rows.

2: Create a mask of missing values $\mathbf{M}$ in the same shape as $\mathbf{X}$, where $\mathbf{M}$ is **true** where $\mathbf{X}$ is missing and **false** where $\mathbf{X}$ is observed. Note that missing values are only present in variables, not in features.

3: Split $\mathbf{X}$ into K clusters $\mathbf{X}^k$ using K-Means algorithm.

4: **for** cluster $k = 1, 2, \ldots, K$ **do**

5:    **while** stopping criterion not reached **do**

6:      **for** variable $v = 1, 2, \ldots, n$ **do**

7:        Define current variable as predictand $\mathbf{y}_v^k$ and all other columns of $\mathbf{X}^k$ as predictors $\mathbf{X}_{-v}^k$.

8:        Define $\mathbf{y}_{v,o}^k$ as all data points in $\mathbf{y}_v^k$ where $\mathbf{M}$ is **false**, and $\mathbf{y}_{v,m}^k$ as all data points where $\mathbf{M}$ is **true**.

9:        Define $\mathbf{X}_{-v,o}^k$ as all data points in $\mathbf{y}_v^k$ where $\mathbf{M}$ is **false** and $\mathbf{X}_{-v,m}^k$ as all data points where $\mathbf{M}$ is **true**.

10:        Fit the regression model $\mathbf{y}_{v,o}^k = f(\mathbf{X}_{-v,o}^k)$ where f denotes the Random Forest method.

11:        Create an updated estimate with the fitted Random Forest $\hat{\mathbf{y}}_{v,m}^k = f(\mathbf{X}_{-v,m}^k)$.

12:        Replace $\mathbf{y}_{v,m}^k$ with the new updated $\hat{\mathbf{y}}_{v,m}^k$ in $\mathbf{X}^k$.

13:        Update stopping criterion.

14:      **end for**

15:    **end while**

16: **end for**

17: Combine all $\mathbf{X}^k$ back to $\mathbf{X}$ and save result.

---

3 Data

To illustrate the impact of fragmented observational records, we focus here on the study of land-climate dynamics. At the land-

245 atmosphere boundary, a complex interplay between soil moisture, temperature and precipitation governs much of the water and energy balance at the surface (Seneviratne et al., 2010). Thus a combination of atmospheric and terrestrial processes influences
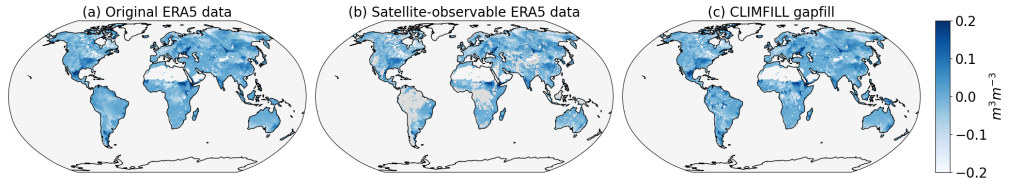
Figure 4. Comparison of (a) the original naturally gap-free ERA-5 reanalysis, (b) the same data but only satellite-observable values are shown, and (c) the gap-fill created from CLIMFILL after starting with the gappy data in (b). The maps show an example snapshot of ERA-5 surface layer soil moisture anomaly on 1 August 2020. CLIMFILL successfully reconstructs major anomalies in surface layer soil moisture for this day. The anomalies are calculated by subtracting the monthly mean values.
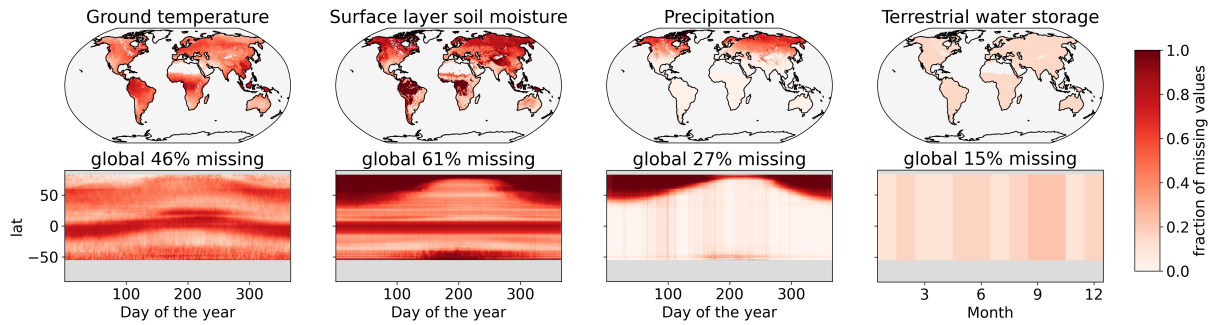
Figure 5. Fraction of missing data in ground temperature from MODIS, ESA-CCI soil moisture, GPM precipitation and GRACE terrestrial water storage observations in the years 2003-2020. Upper panels show fraction of missing data per land points on the ERA-5 grid, lower panels show fraction of missing values per latitude and day of the year. The data are down-sampled to daily values, except GRACE which has monthly resolution.

local climate (Greve et al., 2014; Seneviratne et al., 2010), the development of hot and dry extreme events (Wehrli et al., 2019; Miralles et al., 2019; Mueller and Seneviratne, 2012) or changes freshwater availability (Gudmundsson et al., 2021) and the interaction of all these factors with climate change (Seneviratne et al., 2010). These interactions are inherently multivariate and 250   act on different time scales, making it necessary to observe the variables at a fine spatial and temporal resolution. Consequently, the study of land-climate dynamics requires observations spanning several components of the Earth system, including the land water and energy balances as well as the the atmospheric state.

Since the original values that need to be gap filled are unobserved, we fall back on naturally gap-free atmospheric reanalysis 255   data for benchmarking the framework. We use land-only global reanalysis data from ERA-5 at 0.25 degree resolution for the years 2003-2020 (see Hersbach et al. 2020). ERA-5 is chosen as a gap-free dataset because of its advanced representation of land surface processes (Hersbach et al., 2020) and improved agreement of relevant surface variables with available observations

(Martens et al., 2020; Tarek et al., 2020; Albergel et al., 2018). The missingness patterns of satellite observations in the same period are extracted, regridded to ERA-5 resolution and applied to the corresponding ERA-5 variable. In other words, only the part of the ERA-5 data that would have been observable by satellite are retained. In this "perfect dataset approach", the "true" values of the variables at the locations of the missing values are known and can be compared with the estimates of the gap filling framework (see Figure 4).

The hourly ERA-5 data are aggregated to daily resolution. The aggregation function for each variable is chosen to be consistent with the satellite products (e.g. daily sums for precipitation and daily average for soil moisture, see Appendix Table A1). Since GRACE is only available in monthly resolution, we up-sample the data by linearly interpolating the monthly values to daily resolution. Permanently glaciated areas and deserts (defined as areas with less 50 mm average yearly precipitation in the years 2003-2012) are masked. We extract the missingness pattern from four satellite remote sensing datasets related to land climate interactions and apply it to the ERA-5 dataset: ESA-CCI surface layer soil moisture (Gruber and Scanlon, 2019; Dorigo et al., 2017; Gruber et al., 2017), MODIS ground temperature (Wan et al., 2015), GPM precipitation (Huffmann et al., 2019) and GRACE terrestrial water storage (Swenson, 2012; Landerer and Swenson, 2012; Swenson and Wahr, 2006). These variables represent central interactions between soil moisture and climate that drive land water and energy balance through the soil moisture-temperature and the soil moisture-precipitation feedbacks (Seneviratne et al., 2010). Selecting both microwave remote sensing measures of surface layer soil moisture and total water storage of the land surface is a compromise aiming at including as much possible information of root zone soil moisture as there is available via remote sensing.

There are ubiquitous missing values in the selected satellite observations (Figure 5). Since the missingness patterns are only partially overlapping, the selected set of variables is a good candidate for mutual gap filling. Ground temperature is missing where there is cloud cover, with the maximum of missing values in the inner tropics and extratropical strom tracks, moving along latitudinal bands throughout the year. Almost half of the values globally (46%) of ground temperature are missing in the considered years. Surface layer soil moisture is only observed in 39% of all cases. It is missing where there is ice or snow cover or when vegetation is too dense. This is the most complicated missingness case, because it exhibits the highest fraction of missing values and has considerable amount of land mass where high vegetation cover prevents retrieval at all times. For precipitation, around a quarter of the values are missing (27%), and only in high latitudes during winter. In the GPM remote sensing precipitation dataset values in the presence of surface snow or ice are masked because of poor sensor quality (Huffmann et al., 2019). In postprocessing, Huffmann et al. (2019) use a sophisticated kalman-smoother time interpolation to fill the gaps from the retrieval. From available metadata, we retrieved the originally missing maps to be able to quantify the added value of mutual gap filling for precipitation. Terrestrial water storage is missing if the global measurement is discarded due to instrument failure or during calibration missions (Landerer, 2021), leading to individual months missing, and only 15% missing values.

Table 1. Overview over the individual experiments conducted.

experiment name	Section	included features	years	missingness	fraction of missing values
A: interpolation	4.1	–	2003	real	variable-dependent
B: 4-var	4.1	only the 4 variables	2003	real	variable-dependent
C: embedded	4.1	4 variables + embedded features	2003	real	variable-dependent
D: all	4.1 + 4.2 + 4.3	4 variables + embedded features + constant features	2003-2020	real	variable-dependent
E: MCAR	4.2	4 variables + embedded features + constant features	2003	random	{0.05,0.1,0.2,0.3,...,0.9}
F: MAR	4.2	4 variables + embedded features + constant features	2003	artificial swaths	{0.05,0.1,0.2,0.3,...,0.9}

4 Testing and Benchmarking the CLIMFILL-Algorithm

The results section is structured as follows: Section 4.1 compares CLIMFILL with three different feature sets and the interpolation step (experiments A through D in Table 1). At the end of this section, we settle on a feature set CLIMFILL for the rest of the results. In Section 4.2, the theoretical upper performance-limits given the data described in Section 3 are examined using simpler, artificial missingness patterns and changing fractions of missing values (experiments D, E and F in Table 1). Finally in Section 4.3, CLIMFILL is run for the whole period (2003-2020) (experiment D) and its gap filling results are compared to the original, gappy part of the data that is observable by satellite.

4.1 Benchmarking against univariate interpolation

The objective of the CLIMFILL framework is to not only reconstruct variables separately, but to recover multivariate dependencies. In this first part of the results, we illustrate the improvement of the multivariate gap filling framework CLIMFILL compared to the univariate interpolation that takes place in the first step of the framework (experiment A). With this analysis, we can quantify the added value of incorporating information from the other variables present, which happens in step 4 of the framework. Furthermore within this section, we examine which subset of features created in step 2 is most descriptive for the problem at hand. This is done to ensure an informed decision on the set of features is taken that reflects their usefulness in the gap-filling process. We try three different sets of features: (1) only the four variables (experiment B), (2) the variables plus their embedded features as described in Section 2.2 (experiment C) and (3) all the features created in step 2, including the constant features describing land properties (experiment D). The benchmarking process therefore quantifies the merit of CLIMFILL compared to univariate interpolation and explores the possible feature space for combinations that improve the results.

To allow for a quantitative assessment of the similarity of the multivariate distributions of observed and simulated variables, we apply a scalar measure of multivariate similarity. In this study, we use the Jenson-Shannon distance (JS-distance) (Lin, 1991). This measure compares the distance between two multivariate distributions, where a value of zero means that both distributions are identical, and one indicates that the distributions are not overlapping. We apply the JS-distance on four-
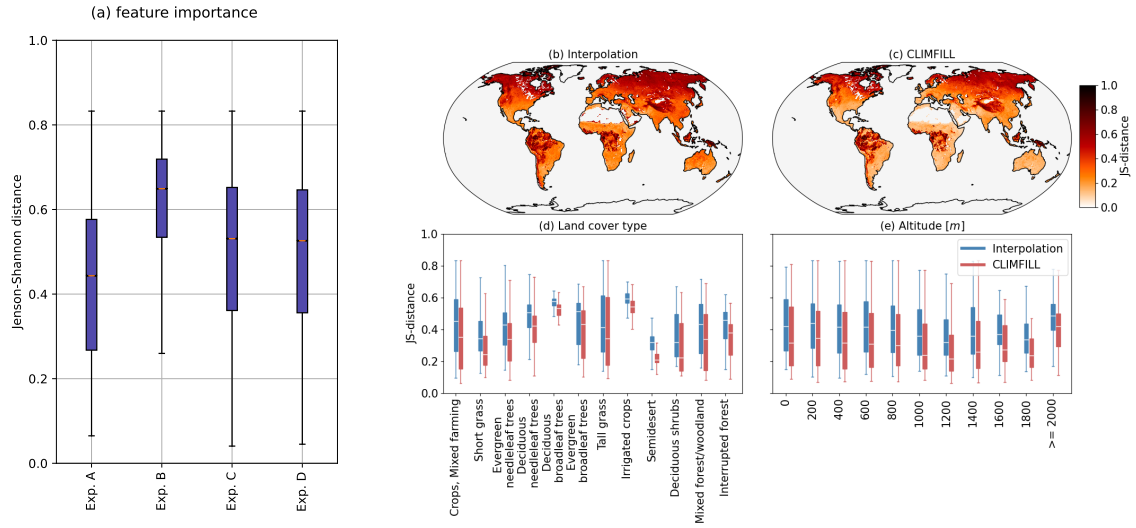
Figure 6. Multivariate JS-distance for interpolation and CLIMFILL gap fill. (a) Boxplots of JS-distance between original ERA-5 data and Interpolation as well as all sets of features as described in Sect. 2.2. (b) Map of JS-distance of univariate interpolation and (c) CLIMFILL considering the multivariate distribution of all variables. (d) JS-distance per land cover type and (e) altitude for interpolation gap-fill and CLIMFILL gap-fill. Land cover type and altitude are extracted from ERA-5. Boxplots show the median as white line, the box as the quartiles and the whiskers at 1.5 times of the quartile length over all landpoints with the specified land cover type or altitude, respectively.
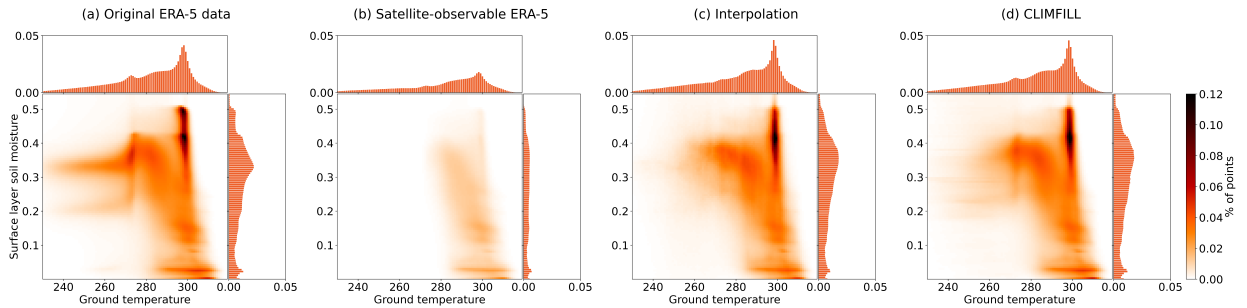
Figure 7. Bivariate and univariate histograms of surface layer soil moisture and ground temperature in (a) original ERA-5 data, (b) the subset of the original ERA-5 data that would have been observable by satellite, (c) gap filled throught univariate interpolation and (d) with CLIMFILL gap filling. For bivariate distributions of other variable pairs see Appendix Figure A1

dimensional histograms computed of the four variables using 50 bins for each variable.

315

Figure 6 shows the JS-distance between the original ERA-5 data and the interpolation as well as the different feature sets. Overall, the JS-distance is lower for CLIMFILL than for interpolation globally (Fig. 6 (a)) for experiment C and D. Adding the constant maps to the feature set leads to a negligible performance improvement. However, including all variables shows overall
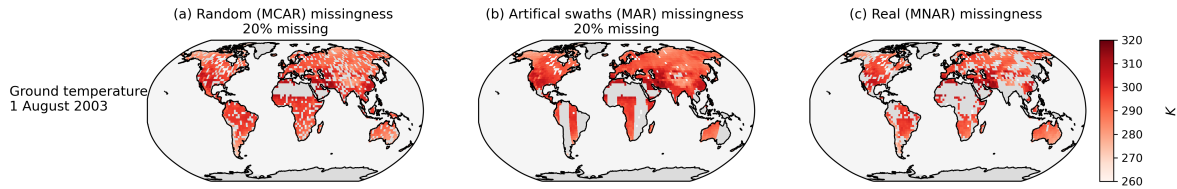
Figure 8. Comparison of artificial (a) random and (b) swaths-only missingness and (c) missingness in the real data in an example snapshot of ERA-5 ground temperature on 1st of August 2003. Random missingness was created by randomly sampling without replacement from the pool of all gridpoints on land at all timesteps in the desired fraction of missing values. In swaths-only missingness we create long ellipses centered around the equator to simulate characteristic satellite swath missingness patterns. Note that the two missingness patterns are not exactly the same for each day and variable to allow for cross-variable learning.

the best results. In the rest of the paper, we will therefore refer to experiment D when referring to CLIMFILL. Regionally, the largest improvement between CLIMFILL and the interpolation is in tropical and subtropical regions (Fig. 6 b, c), where a high fraction of missing values inhibits the performance of interpolation. Taking a closer look at the results by dividing the global map into types of vegetation and altitudes (Fig. 6 d, e) shows that the JS-distance improves from interpolation to CLIMFILL for all altitudes and all land cover types. This indicates an improvement of multivariate features in CLIMFILL gap-fill globally for a wide range of environmental conditions. Overall CLIMFILL has a higher skill in reconstructing the multivariate dependence structure of the original ERA-5 data compared to univariate interpolation.

To illustrate the complex impacts of missing values and their alleviation in univariate and multivariate gap filling, Figure 7 exemplary shows the bivariate distribution of surface layer soil moisture and ground temperature globally for the whole time period (all other possible combinations of variables are shown in Appendix figure A1). The part of the data that is observable from space (Figure 7 b) show a collapsed distribution and clearly fails to recover the original bivariate distribution. Results after univariate interpolation recover parts of the distributions. CLIMFILL furthermore improves this and recovers the shape of the original distribution. Thus it generally provides an improved estimate of the bivariate distribution of surface layer soil moisture and ground temperature such that it is closest to the original ERA-5 data, in spite of knowing only satellite-observable points.

4.2 Data-constrained upper performance limits

Missing values in Earth observation data are often present in a large proportion and a complex MNAR pattern. These characteristic properties of Earth observation data can hamper gap filling. We therefore are interested in exploring the envelope of data properties in which gap filling can be successful and see the deterioration of performance with increasing data sparsity and increasingly complex missing value patterns. In contrast to the last section, the goal is to show the upper limit of what is
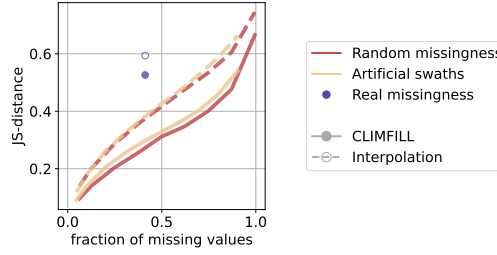
Figure 9. Median performance of gap filling with CLIMFILL and univariate interpolation on different missingness patterns and fractions of missingness expressed in JS-distance (for more detail see text) per variable. Gap filling for random missingness and artifical swaths is executed for a range of fraction of missing values and denoted as a line, while real missingness is only one case depicted as point. The metrics are calculated over each timestep for all not satellite-observable values of gridpoints on land and the median of all landpoints is plotted.
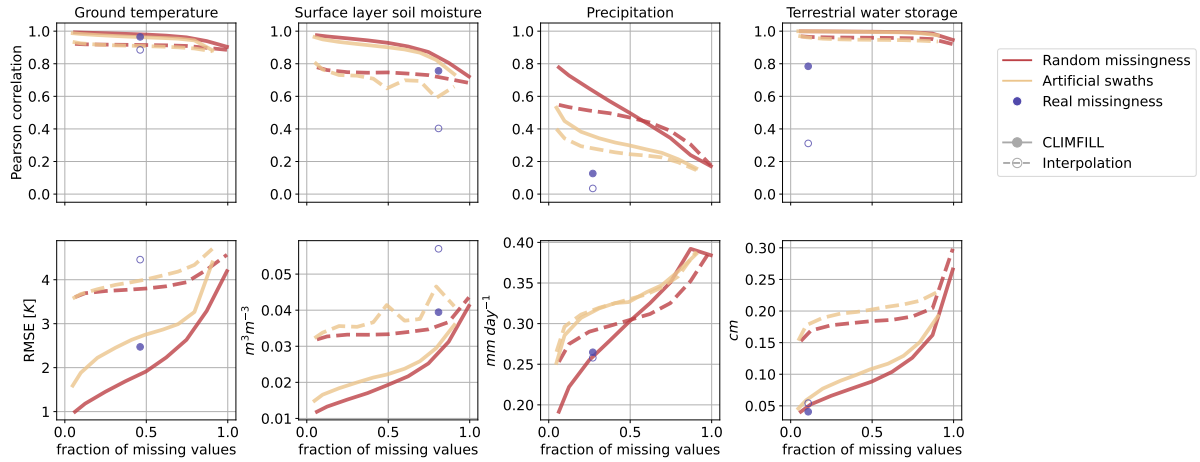
Figure 10. Median performance of gap filling with CLIMFILL and univariate interpolation on different missingness patterns and fractions of missingness expressed in two metrics: Pearson correlation and Root Mean Square Error (RMSE) per variable. Gap filling for random missingness and artifical swaths is executed for a range of fraction of missing values and denoted as a line, while real missingness is only one case depicted as point. The metrics are calculated over each timestep for all not satellite-observable values of gridpoints on land and the median of all landpoints is plotted.

possible in gap filling with the complex missingness patterns exhibit by satellite observations. To this end we rely on the four considered variables to test the impact of increasing fractions of missing data using idealised patterns. In particular, we delete (1) data according to a MCAR random missingness pattern (experiment E, Fig 8 a) and (2) by imitating satellite swaths, effectively creating MAR missingness patterns (experiment F, Fig. 8 b). Both patterns are applied for fractions of missing values 345 between 5% to 95% for each of the variables.

Multivariate JS-distance (Figure 9) and univariate statistical performance measures (Figure 10) are used to compare original and gap filled values for all performed experiments. With increasing fraction of missing values, the two artificial missingness cases increase in error, increase in their JS-distance and decrease in correlation. Once more than 80% of the values are missing, the gap filling breaks down because not enough observed values are available for the iterative procedure to converge to a meaningful result. Random and artificial swath missingness show similar deterioration with increasing fraction of missing values, but values missing completely at random tend to be easier to estimate at all fractions of missing values. Gap filling random missingness is the easiest case, since it is likely that neighboring or environmentally similar points are observed. MAR missingness exposes large patches of missing values, making spatiotemporal interpolation less effective and hence decreasing the gap filling performance as compared to MCAR. Since the real (MNAR) missingness case is the most complex missingness pattern, these additional experiments serve as upper limits of the performance in the real case.

When moving from the artificial patterns of missingness to the real case (dots and circles in Fig. 9 and Fig. 10), the deterioration in performance is different for each of the variables. However, in most cases the metrics for the real missingness case are close to the artificial missigness patterns, suggesting CLIMFILL operates at the upper limit of what is possible with the complex missingness pattern of real observations. For ground temperature, a spatially and temporally smooth variable, the interpolation is already quite a good first guess, its correlation is only slightly improved in CLIMFILL. However, the RMSE drops quite dramatically, indicating smaller biases in ground temperature for gap filled data. In this case study, we found the biggest improvement compared to interpolation for surface layer soil moisture despite its large fraction of missing values. This high performance could be due to the fact that surface layer soil moisture exposes missingness in areas where other variables are observed, for example in the tropical forests, such that learning in this area is easier. Additionally, variable selection is centered around soil moisture, and soil moisture is a key variable of land hydrological processes. The most difficult case is precipitation. Precipitation estimates are only slightly improved with CLIMFILL compared to initial interpolation. Precipitation is influenced by several processes that are not captured within the four selected variables. For example, frontal rain patterns are mostly not explained by land surface properties but are governed by large scale circulation. This is a challenging case and could still furthermore be improved, for example by adding wind patterns to capture more synoptic features. Terrestrial water storage contains only a small fraction of missing values (15%). Since the interpolation is only applied spatially, it fails for full months of missing data and therefore the difference in correlation between interpolation and CLIMFILL is particularly high.

4.3 Recovery of regional and local land-climate dynamics

For any gap filling framework to be useful for both scientific and practical applications it needs to be able to recover essential properties of the phenomena of interest. The coupling of energy and water between land and atmosphere at the land surface is a central, multivariate property of land climate interactions that is currently underestimated in satellite data (Hirschi, 2014). By comparing CLIMFILL gap-fill with the subset of data that can be observed from space, i.e. the gappy ERA-5 data (Fig. 4) we explore the role of missing values in this problem. This analysis is conducted on the whole available time period 2003-2020 (experiment D). In particular we show that leaving gaps in satellite data unfilled leads to biases and noise in estimates of re-
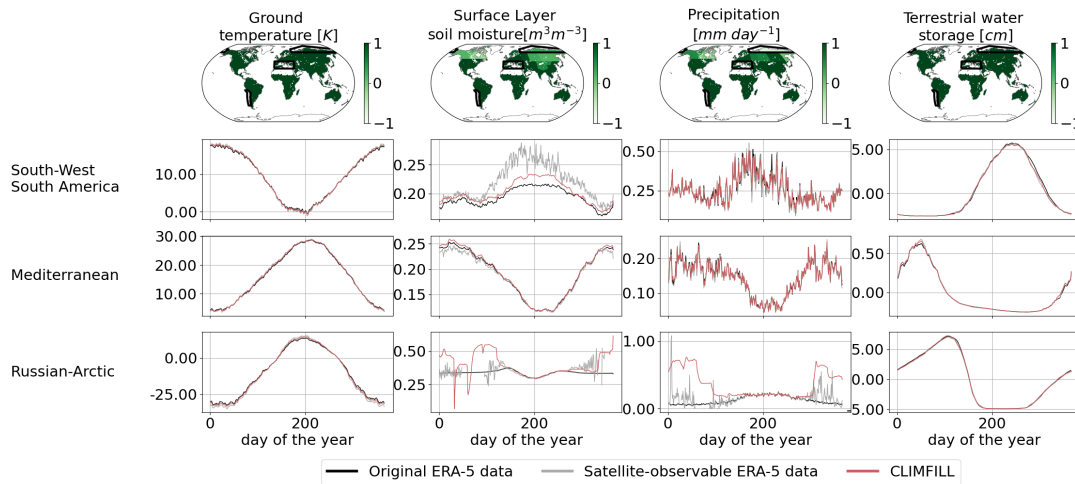
Figure 11. Pearson correlation of regionally averaged mean seasonal cycles between CLIMFILL and the original ERA-5 data over IPCC reference regions (AR6 regions, Iturbide et al. 2020) (top panel maps). Regionally averaged mean seasonal cycle of the physical values over selected regions in original ERA-5 data, satellite-observed ERA-5 data and gap filled CLIMFILL data (bottom panels). The selected regions show exemplary advantages and problems of the framework, see text. For all other AR6 regions see Appendix Fig. A2.

gional and local climate feedbacks and how the CLIMFILL framework can contribute to overcoming this issue.

Figure 11 showcases the pearson correlation between the mean seasonal cycle in original ERA-5 data and CLIMFILL estimates as well as spatial averages of the variables for selected IPCC reference regions (AR6 regions, see Iturbide et al. 2020).

385   Overall we find good agreement between them for the majority of regions in the world. The missing values in the satellite-observable ERA-5 data result in a noisy signal and biased values in regional estimates from the satellite-observable data. CLIMFILL alleviates the noise, reduces the bias and has a high correlation to original ERA-5 data for a majority of regions (for all other regions see Appendix Fig. A2). However, surface layer soil moisture and precipitation suffer from gap filling artefacts in high latitude regions.

390

In Figure 12 the reconstruction of month to month variability by CLIMFILL is shown. Plotted are monthly, deseasonalised anomalies of the four variables for years 2003-2020 as spatial averages for selected IPCC reference regions (for all other regions see Appendix Fig. A5). CLIMFILL overall is able to reconstruct the variability throughout the years. Again here, the skill for surface-layer soil moisture and precipitation estimates is region-dependent. High latitude regions show decreased cor-

395   relation compared to other regions and unrealistic values in winter.
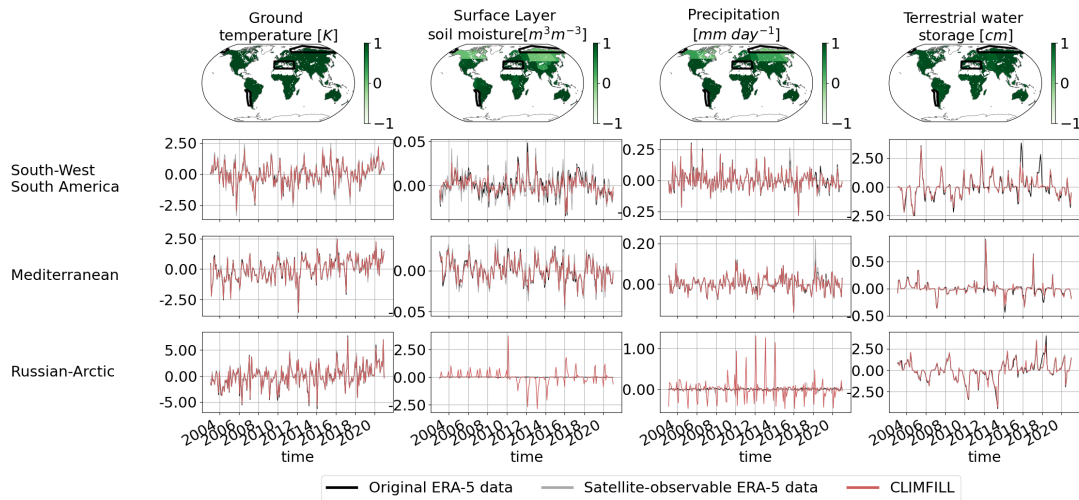
Figure 12. Pearson correlation of regionally averaged, deseasonalised monthly averages between CLIMFILL and the original ERA-5 data over IPCC reference regions (AR6 regions, Iturbide et al. 2020) (top panel maps). Regionally averaged monthly averages of the physical values over selected regions in original ERA-5 data, satellite-observed ERA-5 data and gap filled CLIMFILL data (bottom panels). The selected regions show exemplary advantages and problems of the framework, see text. For all other AR6 regions see Appendix Fig. A5.

The reason the performance of CLIMFILL in high latitude regions in winter can be explained by several reasons. Firstly, precipitation gap filling is a challenging case due to its non-normal distribution. Secondly, soil moisture of frozen soil is hard to define. Thirdly, both variables suffer from unrealistic estimates of the interpolation step. These estimates that are created when the thin-plate-spline interpolation interpolates over areas where observed values are sparse and geographically far away, for example in the Russian Arctic during winter. These unrealistic values cannot fully be dampened by the iterative procedure in step 4 of CLIMFILL. Furthermore, precipitation is a challenging case due to its non-normal distribution. In future versions of the framework, a way to reduce this problem would be to not allow thin-plate-spline interpolation to estimate missing values too distant from observations, and instead rely on regional averages as an initial guess. In summary, for most variables in most regions CLIMFILL shows high correlation with original values and reduces bias and noise of estimates compared to only satellite-observable data for both the seasonal cycle and interannual variability, with some difficulties arising from the missingness patterns of surface layer soil moisture and precipitation in high latitude regions.

Soil moisture-temperature coupling plays an important role for the development of heat extremes (Wehrli et al., 2019; Vogel et al., 2017; Seneviratne et al., 2010). As a last measure, we look at the case study of the European 2003 heat wave. Figure 13 shows the regionally averaged development of ground temperature and surface layer soil moisture for the first 8 months of 2003 as well as anomaly maps of ground temperature for JJA 2003 and surface layer soil moisture for MAM 2003 for the three
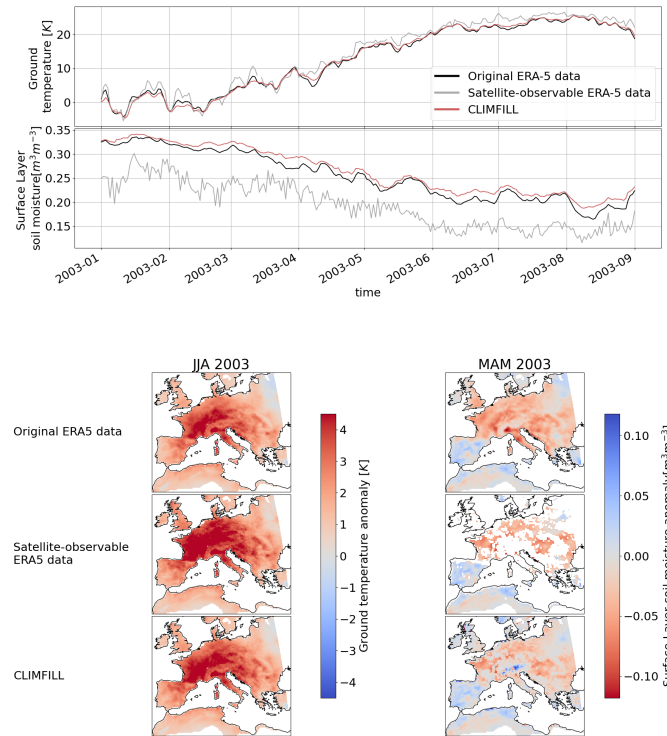
Figure 13. Top: Development of ground temperature and surface layer soil moisture over central Europe from January to August 2003, depicting the European heatwave 2003 for ERA-5 original data, satellite-observable ERA-5-data and CLIMFILL gap-fill. Maps show anomalies of ground temperature for the three cases in JJA 2003 and anomalies of surface layer soil moisture in the three preceeding months (MAM 2003) over Europe.

cases. With satellite-observable data only, the ground temperature is overestimated, because only clear-sky values are reported and ground temperature values below clouds, usually systematically lower during daytime in summer, are missing. CLIMFILL alleviates this bias and brings absolute temperatures and anomalies close to the original ERA-5 data. A strong dry soil moisture anomaly in spring was characteristic for the 2003 heat event, which is overestimated and noisy in the satellite-observable data. CLIMFILL is able to recover the spatial distribution of the event and reduce the bias. The 2003 heat wave is showcasing how CLIMFILL can alleviate biases and noise and show a more realistic heat extreme development compared to gappy satellite data.

5   Discussion and conclusions

Gaps in remotely-sensed Earth observations are ubiquitous, unavoidable and lead to a fragmented record of observational data. Ignoring these gaps creates noisy and biased derived statistics and regional averages. Spatial, univariate interpolation with state-of-the-art methods do typically only consider one variable at a time and can therefore not fully recover the multivariate dependence structure between the variables. To bridge this gap, a framework for gap filling multivariate gridded Earth observations, CLIMFILL, is proposed. CLIMFILL estimates missing values by not only considering spatial and temporal but also the multivariate dependence across variables. In doing that CLIMFILL mines the highly structured nature of geoscientific datasets and combines interpolation-centered approaches common to geosciences and multivariate gap filling methods from statistical literature. In contrast to popular up-scaling approaches, CLIMFILL does not need a gap-free gridded "donor" variable for estimating missing values. Thus the algorithm and can digest complex patterns of missigness in multivariate Earth observations. CLIMFILL fills gaps in fragmented Earth Observations while recovering the physical dependence structure among the considered variables. To this end, the CLIMFILL framework contributes to decreasing the inherent fragmentation of Earth observations, enables usage of multiple gappy satellite observations simultaneously and is a helpful tool when working towards a coherent digital representation of the Earth.

This study illustrates the need for gap filling approaches and the merit of CLIMFILL with a set of variables relevant for the study of land-climate dynamics. CLIMFILL is benchmarked in an exemplary setting of reanalysis data with focus on variables relevant for the study of land-climate dynamics. To this end, reanalysis data have been deleted to match missing values in satellite observations in a "perfect dataset approach". The multivariate JS-distance shows that CLIMFILL recovers the dependence structure in the considered variables. Furthermore, univariate metrics show that CLIMFILL estimates have better agreement to original ERA-5 data compared to gappy data for many variables and regions. In summary, CLIMFILL is able to recover the dependence structure among several variables, in contrast to results obtained when missing values are not gap filled.

Although in this case study only four variables are considered, which high in their respective fraction of missing values (up to more than two thirds of the values missing) and complex in their pattern of missing values (always missing not at random), the multivariate gap filling with CLIMFILL improves estimates compared to univariate spatial interpolation. This is likely explained by the high correlation among the variables, which can to some degree counteract the complex missingness. This highlights that information from other physically relevant available variables can be beneficial for gap filling, indicating that the power of the framework might increase if even more dependent are included. Idealised experiments with simpler missingness patterns and different fractions of missing values within these four variables show that CLIMFILL improves upon univariate interpolation in all cases for all considered metrics, and the performance is close to easier cases with less complex missingness patterns for most variables.

In short, we have presented CLIMFILL, a multivariate gap filling framework that exploits spatial, temporal and multivariate information to create estimates for missing values in Earth observations. The fidelity of the framework has been successfully demonstrated in a case study centered around remote sensing observations relevant for the study of land-climate dynamics, which highlighted the the merits of the approach compared to univariate interpolation. It is nevertheless important to stress that the "perfect dataset" approach employed here for benchmarking might not be fully representative for real observations. Therefore we stress that the fidelity of the suggested algorithm has to be evaluated for real satellite observations and new applications. A natural next step could be to apply this gap filling mechanism on a larger number of relevant observed variables and create a consistent, gap-free reconstruction of land hydrology.

Missing values in Earth observations are ubiquitous. Our efforts should center around reducing these gaps in observations by e.g. enhancing sensors, developing new measurement techniques or closing gaps in observational networks. Looking at the problem from the other end, another approach could be to optimise the current observational capacities for information completeness, for example utilising methods from information theory (Bauer et al., 2021a) and tackle gaps first that are largest or most severe for data analysis, both in natural and physical space. However, missing values will still remain unavoidable in many observations. Where they are present, it is imperative to develop dependable estimates that also consider links among variables. To this end, the CLIMFILL framework, is developed to not only produce dependable estimates of individual variables but also to recover multivariate dependencies, eventually facilitating the creation of gap-free observational data products for environmental monitoring that also enable the study of Earth system processes, allow observation-only process analysis or can help to assimilate relevant but gappy observations into physical models.

Code and data availability. The current version of CLIMFILL is available from the project website: https://github.com/climachine/climfill under the Apache 2.0 License. The exact version of the model used to produce the results used in this paper is archived on Zenodo (https://doi.org/10.5281/zenodo.4773663), as are scripts to run the model and produce the plots for all the simulations presented in this paper. CLIMFILL was written in python (Python Software Foundation, https://www.python.org/) with core packages including xarray (Hoyer et al., 2020), numpy (Harris et al., 2020), matplotlib (Hunter, 2007), scikit-learn (Pedregosa et al., 2011), regionmask (Hauser, 2021) and scipy (Virtanen et al., 2020). The used ERA-5 data are publicly available at: https://www.ecmwf.int/en/forecasts/reanalysis-datasets/era5 (last accessed: 16th February 2021).
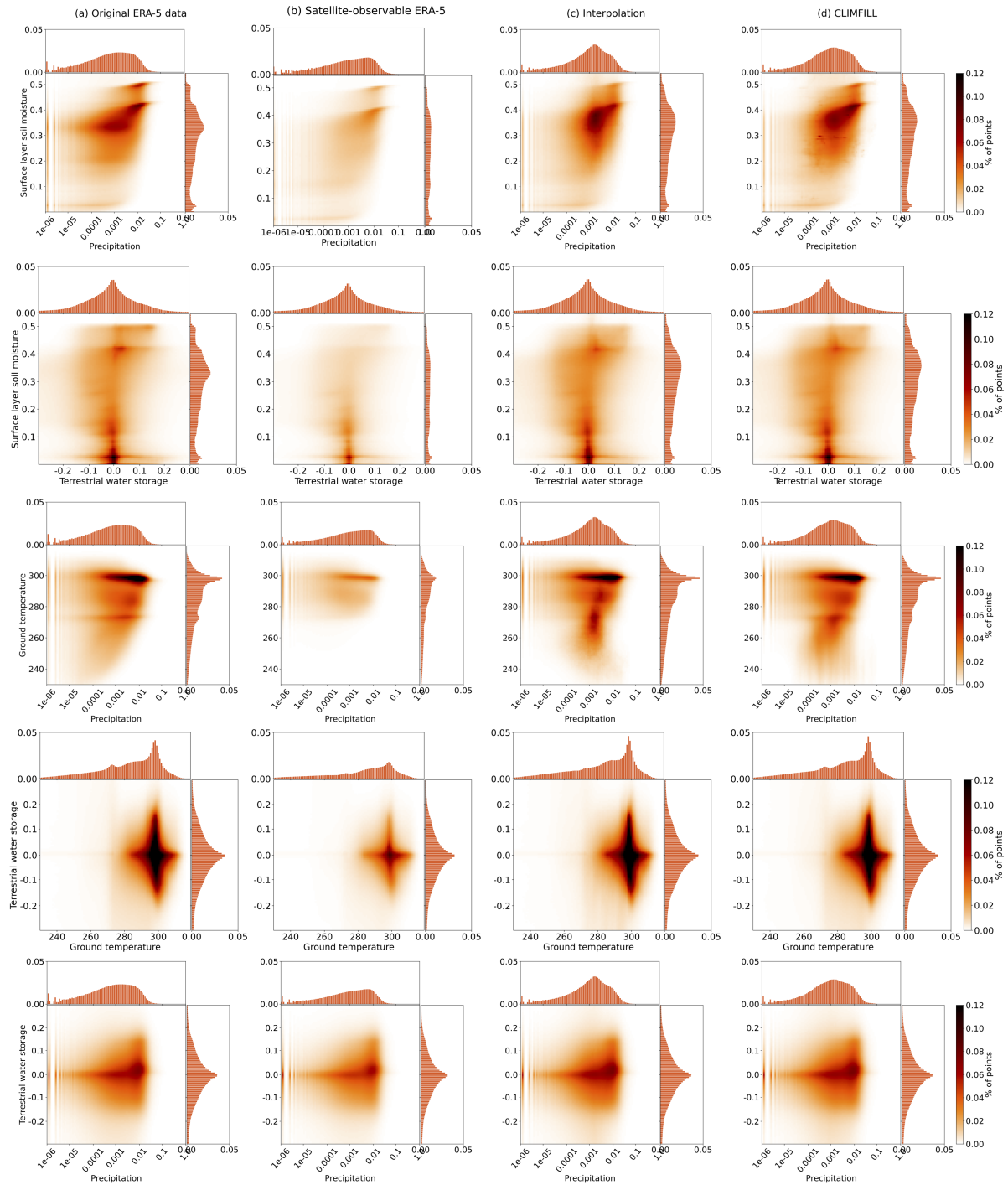
Figure A1. Improvement of multivariate distribution with CLIMFILL gap filling: 2D-histogram for all other combinations of variables (apart from the one already shown in Figure 7) for the original ERA-5 data, satellite-observable ERA-5 data, the Interpolation gapfill and CLIMFILL gapfill.
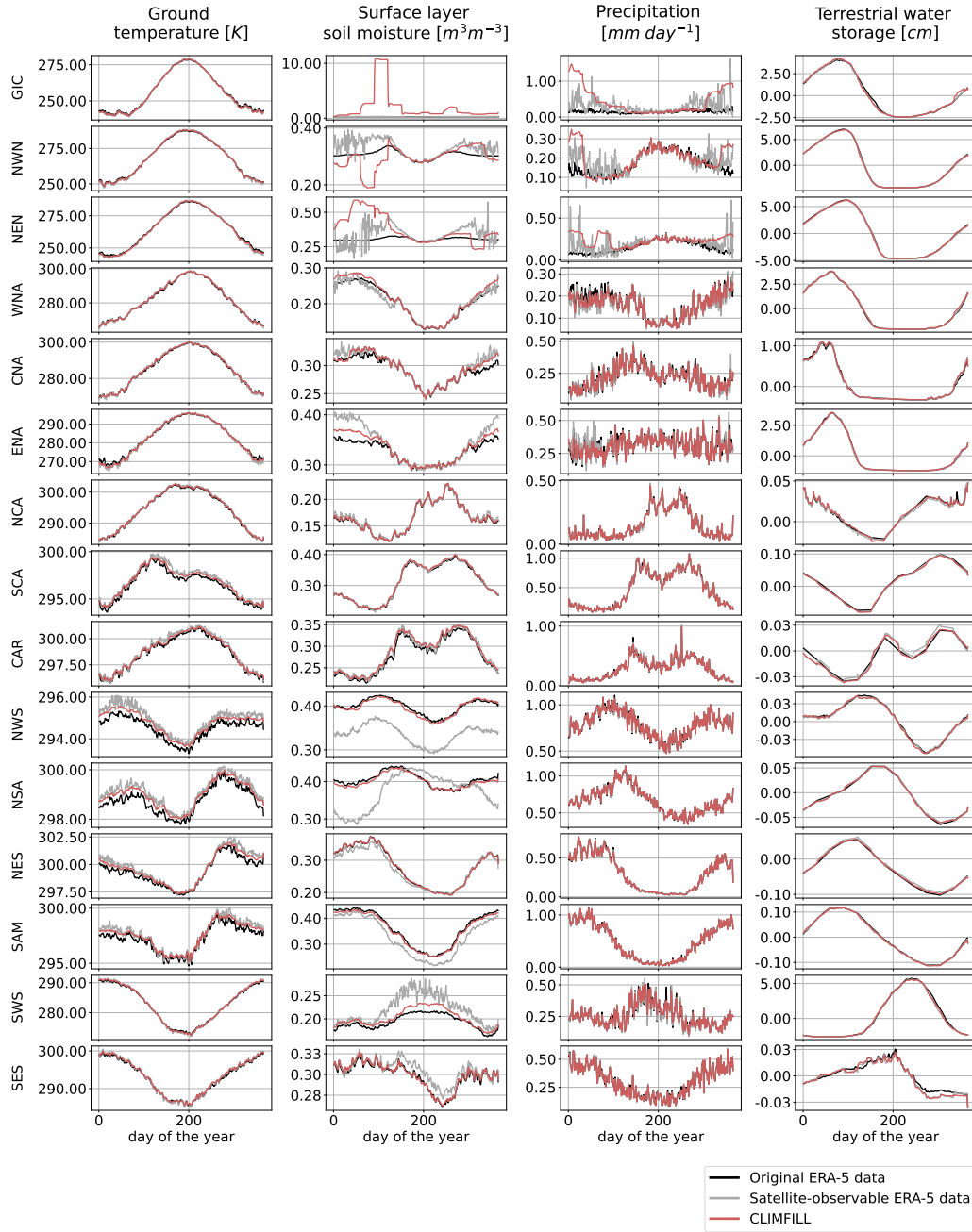
Figure A2. Mean seasonal cycle over all IPCC reference regions on land except Antarctica (AR6 regions, as described in Iturbide et al. 2020) in original ERA-5 data, satellite-observed ERA-5 data and data gap filled with CLIMFILL.
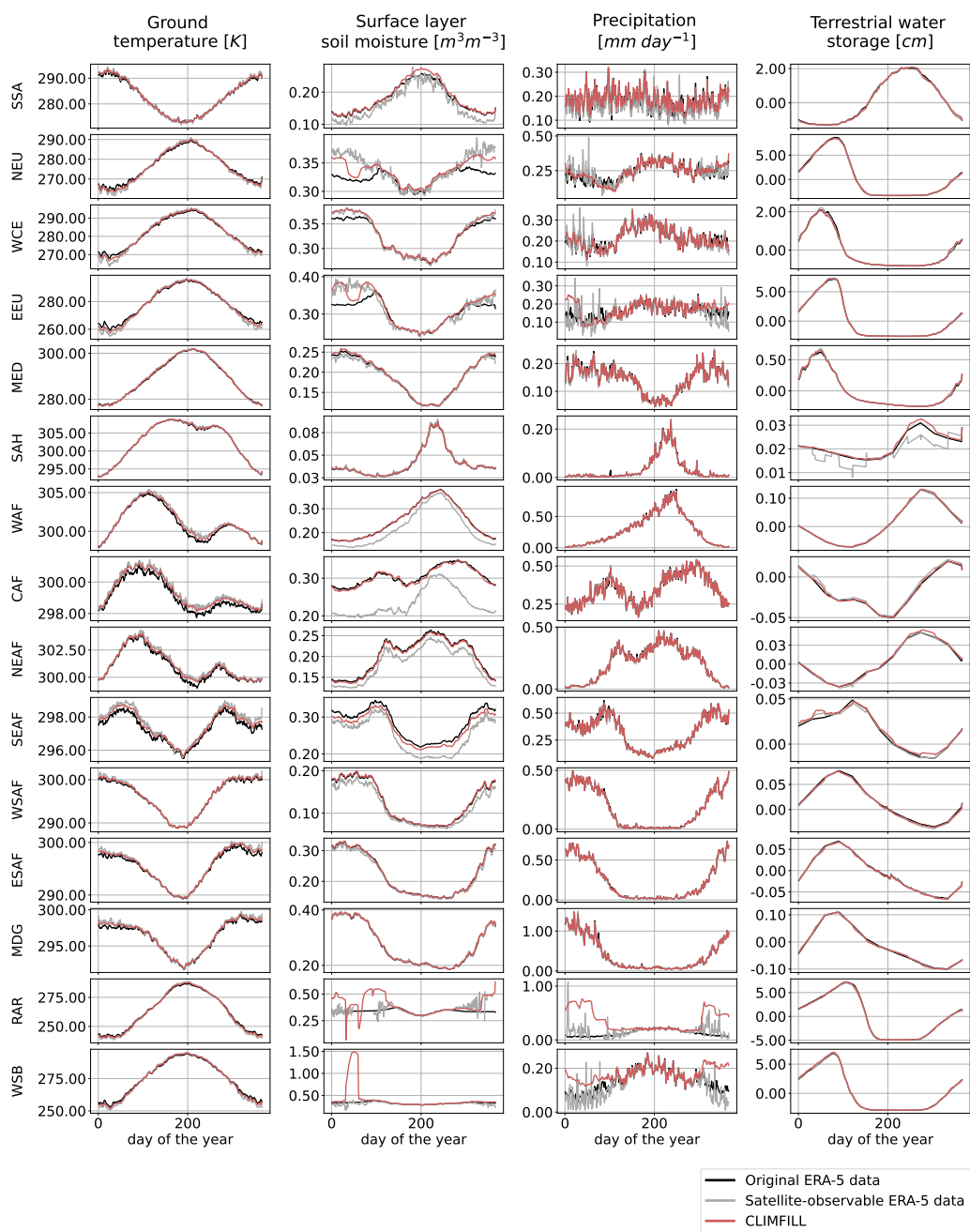
Figure A3. Appendix Figure A2 continued
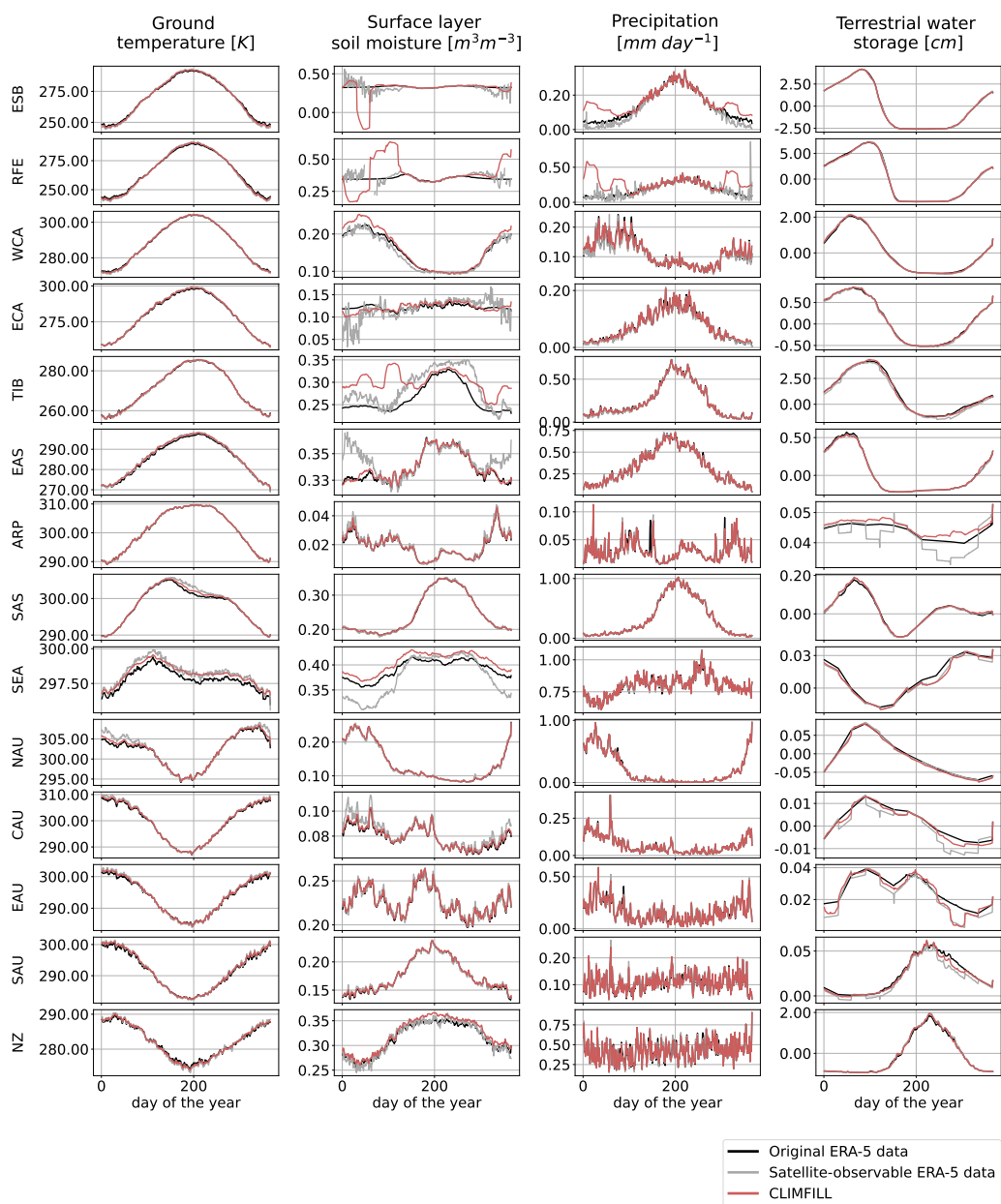
Figure A4. Appendix Figure A2 continued
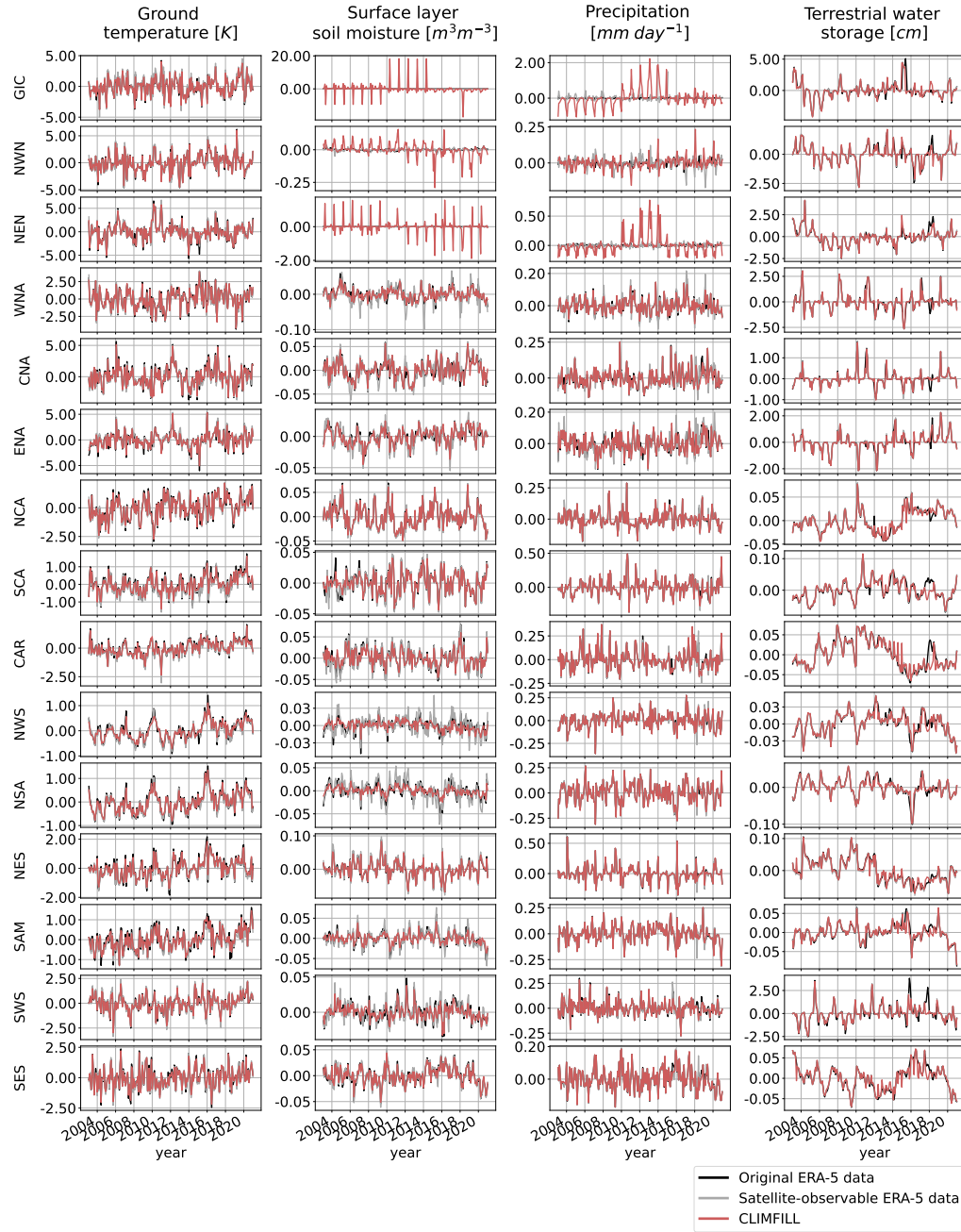
Figure A5. Interannual variability over all IPCC reference regions on land except Antarctica (AR6 regions, as described in Iturbide et al. 2020) in original ERA-5 data, satellite-observed ERA-5 data and data gap filled with CLIMFILL.
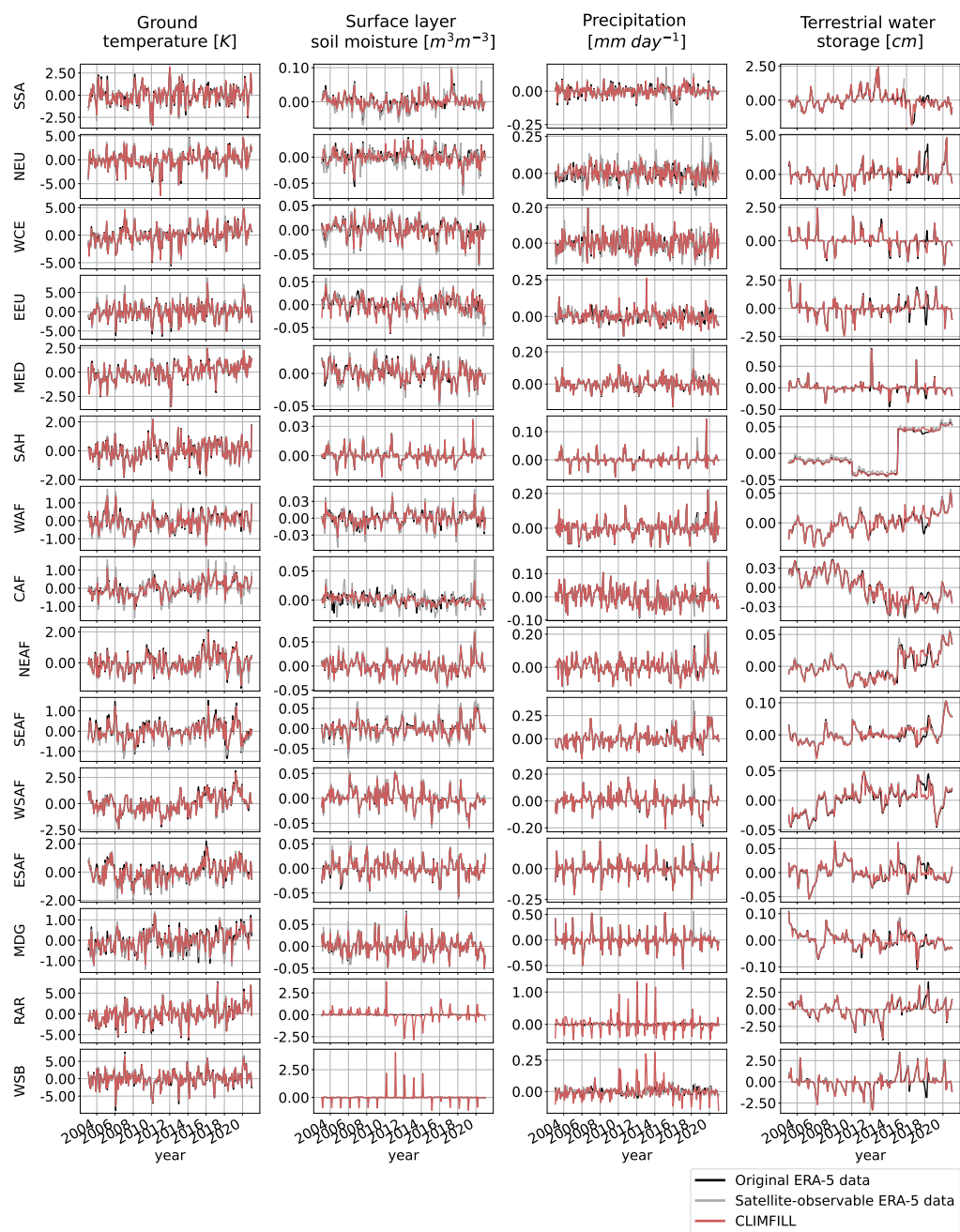
Figure A6. Appendix Figure A5 continued
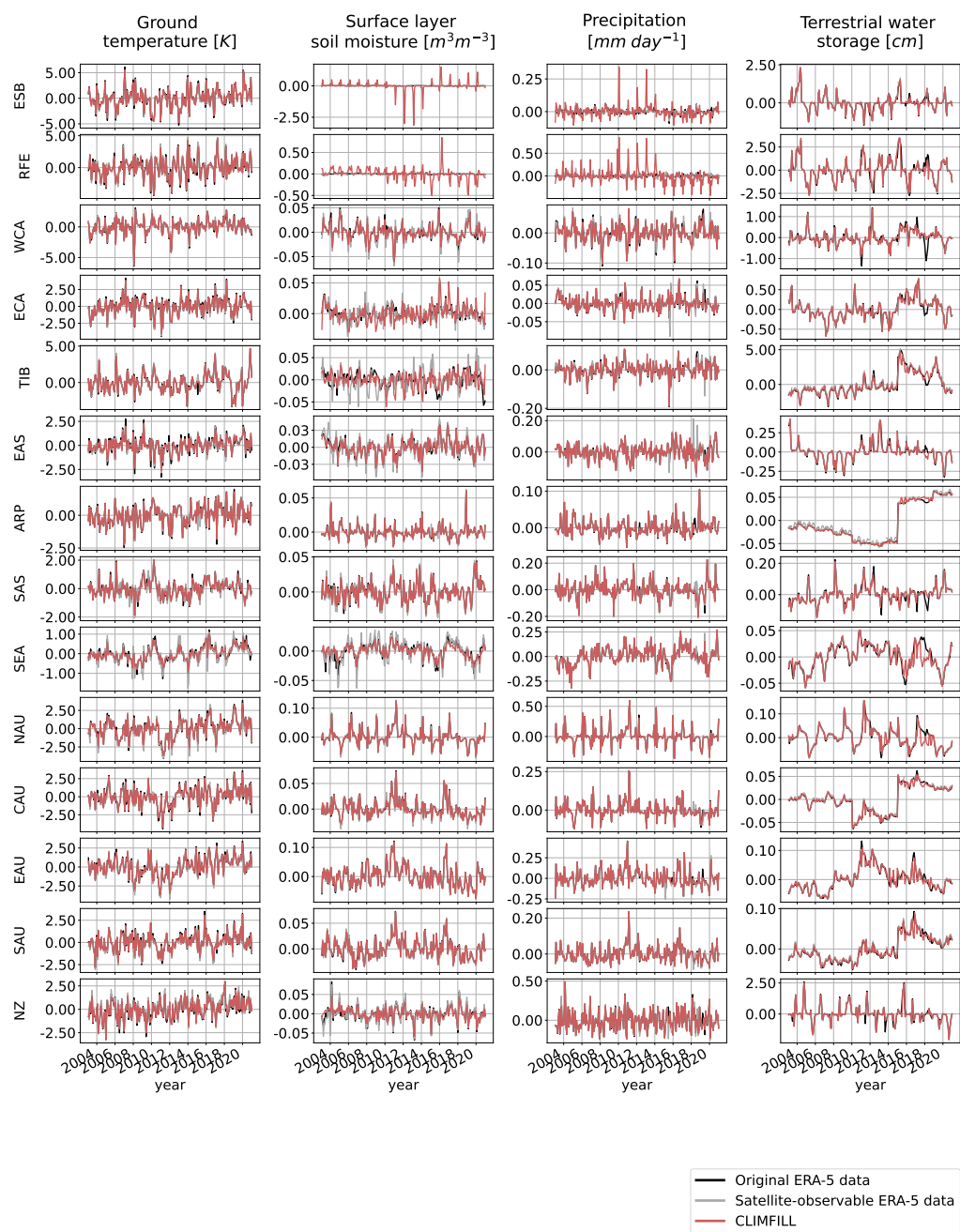
Figure A7. Appendix Figure A5 continued

Table A1. Mapping of ERA-5 variables with satellite observations.

satellite observation	ERA-5 variable	daily aggregation	unit
ESA-CCI surface layer soil moisture	volumetric soil water layer 1 $swvl1$	daily mean	$m^3 m^{-3}$
MODIS ground temperature	ground temperature skt	daily mean	K
GPM precipitation	total precipitation tp	daily sum	$mm\ day^{-1}$
GRACE terrestrial water storage	volumentric soil water layer 1 to 4, snow depth sd and lake cover cl multiplied with lake depth dl	anomalies of daily sums compared to GRACE baseline (2004-2009)	cm (water equivalent thickness)

Table A2. Hyper-parameters of each step, their respective values and how they were determined.

step	hyper-parameter	value	reason
Step 1: Interpolation	number of neighbors in thin-plate-spline interpolation	50	as large as computationally feasible
	smoothing parameter in thin-plate-spline interpolation	variable-dependent	depends on the size of the gaps. large gaps needs larger smoothing parameter to avoid overfitting when extrapolating into empty space
	degree parameter in thin-plate-spline interpolation	2	calibrated on observed cubes in year 2013
	Gaussian Process kernel	variable-dependent	calibrated on observed cubes in year 2013
	number of repeats of Gaussian Process	5	as large as computationally feasible
	number of random points chosen in Gaussian Process	1000	as large as computationally feasible
Step 4: Learning	number of trees	300	as large as computationally feasible
	minimum number of samples in leaf node	2	calibrated on observed cubes in year 2013
	fraction of features used for each split	0.5	as large as computationally feasible
	fraction of datapoints used for each split	0.5	as large as computationally feasible

Author contributions. VB, LG, and SIS designed the study based on an initial idea from LG. VB and LG developed the framework and the evaluation. VB carried out the analysis and drafted the text. All authors contributed to reviewing and editing the article.

Competing interests. The authors declare that they have no conflict of interest.

Acknowledgements. The authors would like to thank Nicolai Meinshausen for input on the initial idea, Mathias Hauser for help in publishing the accompanying python package and Martin Hirschi for post-processing the ERA-5 data. Some of the calculations were performed using the Euler cluster at ETH Zurich. We would like to thank the ECMWF for creating and providing the ERA-5 reanalysis product. We would like to thank Johannes Senn, Joel Zeder, Jonas Jucker and Roberto Villalobos for feedback on the draft. Lastly, we thank the reviewers for their very useful feedback, which greatly helped to improve this study.

References

Albergel, C., Dutra, E., Munier, S., Calvet, J.-C., Munoz-Sabater, J., de Rosnay, P., and Balsamo, G.: ERA-5 and ERA-Interim driven ISBA land surface model simulations: which one performs better?, Hydrology and Earth System Sciences, 22, 3515–3532, https://doi.org/10.5194/hess-22-3515-2018, 2018.

Alemohammad, S. H., Fang, B., Konings, A. G., Aires, F., Green, J. K., Kolassa, J., Miralles, D., Prigent, C., and Gentine, P.: Water, Energy, and Carbon with Artificial Neural Networks (WECANN): a statistically based estimate of global surface turbulent fluxes and gross primary productivity using solar-induced fluorescence, Biogeosciences, 14, 4101–4124, https://doi.org/doi.org/10.5194/bg-14-4101-2017, 2017.

Balsamo, G., Agusti-Panareda, A., Albergel, C., Arduini, G., Beljaars, A., Bidlot, J., Blyth, E., Bousserez, N., Boussetta, S., Brown, A., Buizza, R., Buontempo, C., Chevallier, F., Choulga, M., Cloke, H., Cronin, M. F., Dahoui, M., De Rosnay, P., Dirmeyer, P. A., Drusch, M., Dutra, E., Ek, M. B., Gentine, P., Hewitt, H., Keeley, S. P., Kerr, Y., Kumar, S., Lupu, C., Mahfouf, J.-F., McNorton, J., Mecklenburg, S., Mogensen, K., Muñoz-Sabater, J., Orth, R., Rabier, F., Reichle, R., Ruston, B., Pappenberger, F., Sandu, I., Seneviratne, S. I., Tietsche, S., Trigo, I. F., Uijlenhoet, R., Wedi, N., Woolway, R. I., and Zeng, X.: Satellite and In Situ Observations for Advancing Global Earth Surface Modelling: A Review, Remote Sensing, 10, 2038, https://doi.org/10.3390/rs10122038, 2018.

Banerjee, S., Gelfand, A. E., Finley, A. O., and Sang, H.: Gaussian predictive process models for large spatial data sets, Journal of the Royal Statistical Society: Series B (Statistical Methodology), 70, 825–848, https://doi.org/10.1111/j.1467-9868.2008.00663.x, https://onlinelibrary.wiley.com/doi/10.1111/j.1467-9868.2008.00663.x, 2008.

Bauer, P., Thorpe, A., and Brunet, G.: The quiet revolution of numerical weather prediction, Nature, 525, 47–55, https://doi.org/10.1038/nature14956, 2015.

Bauer, P., Dueben, P. D., Hoefler, T., Quintino, T., Schulthess, T. C., and Wedi, N. P.: The digital revolution of Earth-system science, Nature Computational Science, 1, 104–113, https://doi.org/10.1038/s43588-021-00023-0, http://www.nature.com/articles/s43588-021-00023-0, 2021a.

Bauer, P., Stevens, B., and Hazeleger, W.: A digital twin of Earth for the green transition, Nature Climate Change, 11, 80–83, https://doi.org/10.1038/s41558-021-00986-y, http://www.nature.com/articles/s41558-021-00986-y, 2021b.

Bhattacharjee, S. and Chen, J.: Prediction of Satellite-Based Column CO_2 Concentration by Combining Emission Inventory and LULC Information, IEEE Transactions on Geoscience and Remote Sensing, 58, 8285–8300, https://doi.org/10.1109/TGRS.2020.2985047, https://ieeexplore.ieee.org/document/9094001/, 2020.

Bocquet, M., Brajard, J., Carrassi, A., and Bertino, L.: Data assimilation as a learning tool to infer ordinary differential equation representations of dynamical models, Nonlinear Processes in Geophysics, 26, 143–162, https://doi.org/10.5194/npg-26-143-2019, 2019.

Breiman, L.: Random Forests, Machine Learning, 45, 5–32, https://doi.org/10.1023/A:1010933404324, https://link.springer.com/article/10.1023/A:1010933404324, 2001.

Brocca, L., Ciabatta, L., Massari, C., Moramarco, T., Hahn, S., Hasenauer, S., Kidd, R., Dorigo, W., Wagner, W., and Levizzani, V.: Soil as a natural rain gauge: Estimating global rainfall from satellite soil moisture data, Journal of Geophysical Research: Atmospheres, 119, 5128–5141, https://doi.org/10.1002/2014JD021489, 2014.

Brooks, E. B., Thomas, V. A., Wynne, R. H., and Coulston, J. W.: Fitting the Multitemporal Curve: A Fourier Series Approach to the Missing Data Problem in Remote Sensing Analysis, IEEE Transactions on Geoscience and Remote Sensing, 50, 3340–3353, https://doi.org/10.1109/TGRS.2012.2183137, 2012.

Chiles, J.-P. and Delfiner, P.: Geostatistics: modeling spatial uncertainty, Wiley series in probability and statistics, Wiley, Hoboken, N.J, 2nd ed edn., 2012.

525 Cowtan, K. and Way, R. G.: Coverage bias in the HadCRUT4 temperature series and its impact on recent temperature trends, Quarterly Journal of the Royal Meteorological Society, 140, 1935–1944, https://doi.org/10.1002/qj.2297, 2014.

Cressie, N. and Wikle, C. K.: Statistics for spatio-temporal data, John Wiley & Sons, 2015.

Cressie, N., Frey, J., Harch, B., and Smith, M.: Spatial prediction on a river network, Journal of Agricultural, Biological, and Environmental Statistics, 11, 127–150, https://doi.org/10.1198/108571106X110649, http://dx.doi.org/10.1198/108571106X110649, 2006.

530 Das, S., Roy, S., and Sambasivan, R.: Fast Gaussian Process Regression for Big Data, Big Data Research, 14, 12–26, https://doi.org/10.1016/j.bdr.2018.06.002, https://linkinghub.elsevier.com/retrieve/pii/S2214579617301909, 2018.

Datta, A., Banerjee, S., Finley, A. O., and Gelfand, A. E.: Hierarchical Nearest-Neighbor Gaussian Process Models for Large Geostatistical Datasets, Journal of the American Statistical Association, 111, 800–812, https://doi.org/10.1080/01621459.2015.1044091, https://www.tandfonline.com/doi/full/10.1080/01621459.2015.1044091, 2016.

535 Davenport, M. A. and Romberg, J.: An Overview of Low-Rank Matrix Recovery From Incomplete Observations, IEEE Journal of Selected Topics in Signal Processing, 10, 608–622, https://doi.org/10.1109/JSTSP.2016.2539100, 2016.

de Jeu, R. A. M., Wagner, W., Holmes, T. R. H., Dolman, A. J., van de Giesen, N. C., and Friesen, J.: Global Soil Moisture Patterns Observed by Space Borne Microwave Radiometers and Scatterometers, Surveys in Geophysics, 29, 399–420, https://doi.org/10.1007/s10712-008-9044-0, 2008.

540 Dee, D. P., Uppala, S. M., Simmons, A. J., Berrisford, P., Poli, P., Kobayashi, S., Andrae, U., Balmaseda, M. A., Balsamo, G., Bauer, P., Bechtold, P., Beljaars, A. C. M., van de Berg, L., Bidlot, J., Bormann, N., Delsol, C., Dragani, R., Fuentes, M., Geer, A. J., Haimberger, L., Healy, S. B., Hersbach, H., Hólm, E. V., Isaksen, L., Kållberg, P., Köhler, M., Matricardi, M., McNally, A. P., Monge-Sanz, B. M., Morcrette, J.-J., Park, B.-K., Peubey, C., de Rosnay, P., Tavolato, C., Thépaut, J.-N., and Vitart, F.: The ERA-Interim reanalysis: configuration and performance of the data assimilation system, Quarterly Journal of the Royal Meteorological Society, 137, 553–597, 545 https://doi.org/10.1002/qj.828, 2011.

Dorigo, W., Wagner, W., Albergel, C., Albrecht, F., Balsamo, G., Brocca, L., Chung, D., Ertl, M., Forkel, M., Gruber, A., Haas, E., Hamer, P. D., Hirschi, M., Ikonen, J., de Jeu, R., Kidd, R., Lahoz, W., Liu, Y. Y., Miralles, D., Mistelbauer, T., Nicolai-Shaw, N., Parinussa, R., Pratola, C., Reimer, C., van der Schalie, R., Seneviratne, S. I., Smolander, T., and Lecomte, P.: ESA CCI Soil Moisture for improved Earth system understanding: State-of-the art and future directions, Remote Sensing of Environment, 203, 185–215, 550 https://doi.org/10.1016/j.rse.2017.07.001, 2017.

Gelaro, R., McCarty, W., Suárez, M. J., Todling, R., Molod, A., Takacs, L., Randles, C. A., Darmenov, A., Bosilovich, M. G., Reichle, R., Wargan, K., Coy, L., Cullather, R., Draper, C., Akella, S., Buchard, V., Conaty, A., da Silva, A. M., Gu, W., Kim, G.-K., Koster, R., Lucchesi, R., Merkova, D., Nielsen, J. E., Partyka, G., Pawson, S., Putman, W., Rienecker, M., Schubert, S. D., Sienkiewicz, M., and Zhao, B.: The Modern-Era Retrospective Analysis for Research and Applications, Version 2 (MERRA-2), Journal of Climate, 30, 5419–5454, 555 https://doi.org/10.1175/JCLI-D-16-0758.1, 2017.

Gelfand, A. E. and Schliep, E. M.: Spatial statistics and Gaussian processes: A beautiful marriage, Spatial Statistics, 18, 86–104, https://doi.org/10.1016/j.spasta.2016.03.006, https://linkinghub.elsevier.com/retrieve/pii/S2211675316300033, 2016.

Gerber, F., Jong, R. d., Schaepman, M. E., Schaepman-Strub, G., and Furrer, R.: Predicting Missing Values in Spatio-Temporal Remote Sensing Data, IEEE Transactions on Geoscience and Remote Sensing, 56, 2841–2853, https://doi.org/10.1109/TGRS.2017.2785240, 2018.

560   Ghahramani, Z. and Jordan, M. I.: Learning from Incomplete Data, Tech. rep., Defense Technical Information Center, https://doi.org/10.21236/ADA295618, 1994.

Ghiggi, G., Humphrey, V., Seneviratne, S. I., and Gudmundsson, L.: GRUN: An observations-based global gridded runoff dataset from 1902 to 2014, Earth System Science Data Discussions, pp. 1–32, https://doi.org/https://doi.org/10.5194/essd-2019-32, 2019.

Gramacy, R. B. and Apley, D. W.: Local Gaussian Process Approximation for Large Computer Experiments, Journal of Computational

565   and Graphical Statistics, 24, 561–578, https://doi.org/10.1080/10618600.2014.914442, http://dx.doi.org/10.1080/10618600.2014.914442, 2015.

Greve, P., Orlowsky, B., Mueller, B., Sheffield, J., Reichstein, M., and Seneviratne, S. I.: Global assessment of trends in wetting and drying over land, Nature Geoscience, 7, 716–721, https://doi.org/10.1038/ngeo2247, 2014.

Gruber, A. and Scanlon, T.: Evolution of the ESA CCI Soil Moisture climate data records and their underlying merging methodology, Earth

570   System Science Data, 11, 717–739, https://doi.org/doi.org/10.5194/essd-11-717-2019, 2019.

Gruber, A., Dorigo, W. A., Crow, W., and Wagner, W.: Triple Collocation-Based Merging of Satellite Soil Moisture Retrievals, IEEE Transactions on Geoscience and Remote Sensing, 55, 6780–6792, https://doi.org/10.1109/TGRS.2017.2734070, 2017.

Gudmundsson, L. and Seneviratne, S. I.: Towards observation-based gridded runoff estimates for Europe, Hydrology and Earth System Sciences, 19, 2859–2879, https://doi.org/10.5194/hess-19-2859-2015, 2015.

575   Gudmundsson, L., Boulange, J., Do, H. X., Gosling, S. N., Grillakis, M. G., Koutroulis, A. G., Leonard, M., Liu, J., Müller Schmied, H., Papadimitriou, L., Pokhrel, Y., Seneviratne, S. I., Satoh, Y., Thiery, W., Westra, S., Zhang, X., and Zhao, F.: Globally observed trends in mean and extreme river flow attributed to climate change, Science, 371, 1159–1162, https://doi.org/10.1126/science.aba3996, 2021.

Harris, C. R., Millman, K. J., van der Walt, S. J., Gommers, R., Virtanen, P., Cournapeau, D., Wieser, E., Taylor, J., Berg, S., Smith, N. J., Kern, R., Picus, M., Hoyer, S., van Kerkwijk, M. H., Brett, M., Haldane, A., del Río, J. F., Wiebe, M., Peterson, P., Gérard-Marchant,

580   P., Sheppard, K., Reddy, T., Weckesser, W., Abbasi, H., Gohlke, C., and Oliphant, T. E.: Array programming with NumPy, Nature, 585, 357–362, https://doi.org/10.1038/s41586-020-2649-2, 2020.

Hauser, M.: Regionmask, https://regionmask.readthedocs.io/en/stable/, 2021.

Haylock, M. R., Hofstra, N., Klein Tank, A. M. G., Klok, E. J., Jones, P. D., and New, M.: A European daily high-resolution gridded data set of surface temperature and precipitation for 1950–2006, Journal of Geophysical Research: Atmospheres, 113, D20119,

585   https://doi.org/10.1029/2008JD010201, 2008.

Heaton, M. J., Datta, A., Finley, A. O., Furrer, R., Guinness, J., Guhaniyogi, R., Gerber, F., Gramacy, R. B., Hammerling, D., Katzfuss, M., Lindgren, F., Nychka, D. W., Sun, F., and Zammit-Mangion, A.: A Case Study Competition Among Methods for Analyzing Large Spatial Data, Journal of Agricultural, Biological and Environmental Statistics, 24, 398–425, https://doi.org/10.1007/s13253-018-00348-w, 2019.

Hersbach, H., Bell, B., Berrisford, P., Hirahara, S., Horányi, A., Muñoz-Sabater, J., Nicolas, J., Peubey, C., Radu, R., Schepers, D., Simmons,

590   A., Soci, C., Abdalla, S., Abellan, X., Balsamo, G., Bechtold, P., Biavati, G., Bidlot, J., Bonavita, M., Chiara, G., Dahlgren, P., Dee, D., Diamantakis, M., Dragani, R., Flemming, J., Forbes, R., Fuentes, M., Geer, A., Haimberger, L., Healy, S., Hogan, R. J., Hólm, E., Janisková, M., Keeley, S., Laloyaux, P., Lopez, P., Lupu, C., Radnoti, G., Rosnay, P., Rozum, I., Vamborg, F., Villaume, S., and Thépaut, J.: The ERA5 global reanalysis, Quarterly Journal of the Royal Meteorological Society, 146, 1999–2049, https://doi.org/10.1002/qj.3803, 2020.

595   Hirschi, M.: Using remotely sensed soil moisture for land–atmosphere coupling diagnostics: The role of surface vs. root-zone soil moisture variability, Remote Sensing of Environment, p. 7, https://doi.org/doi.org/10.1016/j.rse.2014.08.030, 2014.

Hoyer, S., Hamman, J., Roos, M., Cherian, D., Fitzgerald, C., Keewis, Fujii, K., Maussion, F., Crusaderky, Kleeman, A., Clark, S., Kluyver, T., Hauser, M., Munroe, J., Nicholas, T., Hatfield-Dodds, Z., Abernathey, R., MaximilianR, Wolfram, P. J., Alexamici, Signell, J., Sinai, Y. B., Helmus, J. J., Mühlbauer, K., Markel, Rivera, G., Cable, P., Augspurger, T., Johnomotani, and Bovy, B.: pydata/xarray: v0.16.2, https://doi.org/10.5281/ZENODO.598201, 2020.

Huffmann, G., Bolvin, D., Braithwaite, D., Hsu, K., Joyce, R., and Xie, P.: Integrated Multi-satellite Retrievals for GPM (IMERG) version 4.4, NASA's Precipitation Processing Center, accessed 1 Oct 2019 ftp://arthurhou.pps.eosdis.nasa.gov/gpmdata/, 2019.

Humphrey, V., Zscheischler, J., Ciais, P., Gudmundsson, L., Sitch, S., and Seneviratne, S. I.: Sensitivity of atmospheric CO_2 growth rate to observed changes in terrestrial water storage, Nature, 560, 628, https://doi.org/10.1038/s41586-018-0424-4, https://www.nature.com/articles/s41586-018-0424-4, 2018.

Hunter, J. D.: Matplotlib: A 2D Graphics Environment, Computing in Science & Engineering, 9, 90–95, https://doi.org/10.1109/MCSE.2007.55, 2007.

Iturbide, M., Gutiérrez, J. M., Alves, L. M., Bedia, J., Cerezo-Mota, R., Cimadevilla, E., Cofiño, A. S., Di Luca, A., Faria, S. H., Gorodetskaya, I. V., Hauser, M., Herrera, S., Hennessy, K., Hewitt, H. T., Jones, R. G., Krakovska, S., Manzanas, R., Martínez-Castro, D., Narisma, G. T., Nurhati, I. S., Pinto, I., Seneviratne, S. I., van den Hurk, B., and Vera, C. S.: An update of IPCC climate reference regions for subcontinental analysis of climate model data: definition and aggregated datasets, Earth System Science Data, 12, 2959–2970, https://doi.org/10.5194/essd-12-2959-2020, 2020.

Jung, M., Reichstein, M., and Bondeau, A.: Towards global empirical upscaling of FLUXNET eddy covariance observations: validation of a model tree ensemble approach using a biosphere model, Biogeosciences, 6, 2001–2013, https://doi.org/10.5194/bg-6-2001-2009, 2009.

Jung, M., Reichstein, M., Margolis, H. A., Cescatti, A., Richardson, A. D., Arain, M. A., Arneth, A., Bernhofer, C., Bonal, D., Chen, J., Gianelle, D., Gobron, N., Kiely, G., Kutsch, W., Lasslop, G., Law, B. E., Lindroth, A., Merbold, L., Montagnani, L., Moors, E. J., Papale, D., Sottocornola, M., Vaccari, F., and Williams, C.: Global patterns of land-atmosphere fluxes of carbon dioxide, latent heat, and sensible heat derived from eddy covariance, satellite, and meteorological observations, Journal of Geophysical Research, 116, G00J07, https://doi.org/10.1029/2010JG001566, 2011.

Jung, M., Koirala, S., Weber, U., Ichii, K., Gans, F., Camps-Valls, G., Papale, D., Schwalm, C., Tramontana, G., and Reichstein, M.: The FLUXCOM ensemble of global land-atmosphere energy fluxes, Scientific Data, 6, 74, https://doi.org/10.1038/s41597-019-0076-8, http://www.nature.com/articles/s41597-019-0076-8, 2019.

Kadow, C., Hall, D. M., and Ulbrich, U.: Artificial intelligence reconstructs missing climate information, Nature Geoscience, 13, 408–413, https://doi.org/10.1038/s41561-020-0582-5, 2020.

Landerer, F.: GRACE & GRACE-FO - Data Months / Days, https://grace.jpl.nasa.gov/data/grace-months/, 2021.

Landerer, F. W. and Swenson, S. C.: Accuracy of scaled GRACE terrestrial water storage estimates, Water Resour. Res., 48, W04 531, https://doi.org/10.1029/2011WR011453, 2012.

Lettenmaier, D. P., Alsdorf, D., Dozier, J., Huffman, G. J., Pan, M., and Wood, E. F.: Inroads of remote sensing into hydrologic science during the WRR era, Water Resources Research, 51, 7309–7342, https://doi.org/10.1002/2015WR017616, 2015.

Lin, J.: Divergence measures based on the Shannon entropy, IEEE Transactions on Information Theory, 37, 145–151, https://doi.org/10.1109/18.61115, http://ieeexplore.ieee.org/document/61115/, 1991.

Little, R. J. A. and Rubin, D. B.: Missing Data in Experiments, in: Statistical Analysis with Missing Data, pp. 24–40, John Wiley & Sons, Ltd, https://doi.org/10.1002/9781119013563.ch2, 2014.

Liu, T., Wei, H., and Zhang, K.: Wind power prediction with missing data using Gaussian process regression and multiple imputation, Applied Soft Computing, 71, 905–916, https://doi.org/10.1016/j.asoc.2018.07.027, 2018.

Mariethoz, G., McCabe, M. F., and Renard, P.: Spatiotemporal reconstruction of gaps in multivariate fields using the direct sampling approach: Reconstruction of gaps using direct sampling, Water Resources Research, 48, https://doi.org/10.1029/2012WR012115, 2012.

Martens, B., Miralles, D. G., Lievens, H., van der Schalie, R., de Jeu, R. A. M., Fernández-Prieto, D., Beck, H. E., Dorigo, W. A., and Verhoest, N. E. C.: GLEAM v3: satellite-based land evaporation and root-zone soil moisture, Geosci. Model Dev., 10, 1903–1925, https://doi.org/10.5194/gmd-10-1903-2017, 2017.

Martens, B., Schumacher, D. L., Wouters, H., Muñoz-Sabater, J., Verhoest, N. E. C., and Miralles, D. G.: Evaluating the land-surface energy partitioning in ERA5, Geoscientific Model Development, 13, 4159–4181, https://doi.org/10.5194/gmd-13-4159-2020, 2020.

Mazumder, R., Hastie, T., and Tibshirani, R.: Spectral Regularization Algorithms for Learning Large Incomplete Matrices, Journal of Machine Learning Research, p. 36, 2010.

Miralles, D. G., Gentine, P., Seneviratne, S., and Teuling, A. J.: Land-atmospheric feedbacks during droughts and heatwaves: state of the science and current challenges, Annals of the New York Academy of Sciences, 1436, 19–35, https://doi.org/10.1111/nyas.13912, 2019.

Mueller, B. and Seneviratne, S. I.: Hot days induced by precipitation deficits at the global scale, Proceedings of the National Academy of Sciences, 109, 12 398–12 403, https://doi.org/10.1073/pnas.1204330109, 2012.

Nicolai-Shaw, N., Gudmundsson, L., Hirschi, M., and Seneviratne, S. I.: Long-term predictability of soil moisture dynamics at the global scale: Persistence versus large-scale drivers, Geophysical Research Letters, 43, 8554–8562, https://doi.org/10.1002/2016GL069847, 2016.

Nicolai-Shaw, N., Zscheischler, J., Hirschi, M., Gudmundsson, L., and Seneviratne, S. I.: A drought event composite analysis using satellite remote-sensing based soil moisture, Remote Sensing of Environment, 203, 216–225, https://doi.org/10.1016/j.rse.2017.06.014, http://www.sciencedirect.com/science/article/pii/S0034425717302729, 2017.

O., S. and Orth, R.: Global soil moisture data derived through machine learning trained with in-situ measurements, Scientific Data, 8, 170, https://doi.org/10.1038/s41597-021-00964-1, http://www.nature.com/articles/s41597-021-00964-1, 2021.

Pastorello, G., Trotta, C., Canfora, E., et al.: The FLUXNET2015 dataset and the ONEFlux processing pipeline for eddy covariance data, Scientific Data, 7, 27, https://doi.org/doi.org/10.1038/s41597-020-0534-3, 2020.

Pedregosa, F., Varoquaux, G., Gramfort, A., Michel, V., Thirion, B., Grisel, O., Blondel, M., Prettenhofer, P., Weiss, R., Dubourg, V., Vanderplas, J., Passos, A., Cournapeau, D., Brucher, M., Perrot, M., and Duchesnay, E.: Scikit-learn: Machine Learning in Python, Journal of Machine Learning Research, 12, 2825–2830, http://jmlr.org/papers/v12/pedregosa11a.html, 2011.

Ridder, N. N., Pitman, A. J., Westra, S., Ukkola, A., Do, H. X., Bador, M., Hirsch, A. L., Evans, J. P., Di Luca, A., and Zscheischler, J.: Global hotspots for the occurrence of compound events, Nature Communications, 11, 5956, https://doi.org/10.1038/s41467-020-19639-3, http://www.nature.com/articles/s41467-020-19639-3, 2020.

Rubin, D. B.: Inference and missing data, Biometrika, 63, 581–592, 1976.

Sahoo, A. K., De Lannoy, G. J., Reichle, R. H., and Houser, P. R.: Assimilation and downscaling of satellite observed soil moisture over the Little River Experimental Watershed in Georgia, USA, Advances in Water Resources, 52, 19–33, https://doi.org/10.1016/j.advwatres.2012.08.007, 2013.

Seneviratne, S. I., Corti, T., Davin, E. L., Hirschi, M., Jaeger, E. B., Lehner, I., Orlowsky, B., and Teuling, A. J.: Investigating soil moisture–climate interactions in a changing climate: A review, Earth-Science Reviews, 99, 125–161, https://doi.org/10.1016/j.earscirev.2010.02.004, 2010.

Shen, H. and Zhang, L.: A MAP-Based Algorithm for Destriping and Inpainting of Remotely Sensed Images, IEEE Transactions on Geoscience and Remote Sensing, 47, 1492–1502, https://doi.org/10.1109/TGRS.2008.2005780, 2009.

Shen, H., Li, X., Cheng, Q., Zeng, C., Yang, G., Li, H., and Zhang, L.: Missing Information Reconstruction of Remote Sensing Data: A Technical Review, IEEE Geoscience and Remote Sensing Magazine, 3, 61–85, https://doi.org/10.1109/MGRS.2015.2441912, 2015.

Stekhoven, D. J. and Bühlmann, P.: MissForest–non-parametric missing value imputation for mixed-type data, Bioinformatics (Oxford, England), 28, 112–118, https://doi.org/10.1093/bioinformatics/btr597, 2012.

Swenson, S. and Wahr, J.: Post-processing removal of correlated errors in GRACE data, Geophysical Research Letters, 33, L08 402, https://doi.org/10.1029/2005GL025285, 2006.

Swenson, S. C.: GRACE Montly Land and Water Mass Grids NetCDF Release 5.0. Ver. 5.0. PO.DAAC, CA, USA., NASA JPL, https://doi.org/https://doi.org/10.5067/TELND-NC005, 2012.

Tang, F. and Ishwaran, H.: Random forest missing data algorithms, Statistical Analysis and Data Mining: The ASA Data Science Journal, 10, 363–377, https://doi.org/10.1002/sam.11348, http://doi.wiley.com/10.1002/sam.11348, 2017.

Tarek, M., Brissette, F. P., and Arsenault, R.: Evaluation of the ERA5 reanalysis as a potential reference dataset for hydrological modelling over North America, Hydrology and Earth System Sciences, 24, 2527–2544, https://doi.org/10.5194/hess-24-2527-2020, 2020.

Teuling, A. J., Seneviratne, S. I., Stockli, R., Reichstein, M., Moors, E., Ciais, P., Luyssaert, S., van den Hurk, B., Ammann, C., Bernhofer, C., Dellwik, E., Gianelle, D., Gielen, B., Grunwald, T., Klumpp, K., Montagnani, L., Moureaux, C., Sottocornola, M., and Wohlfahrt, G.: Contrasting response of European forest and grassland energy exchange to heatwaves, Nature Geosci, 3, 722–727, https://doi.org/10.1038/ngeo950, http://dx.doi.org/10.1038/ngeo950, 2010.

Tramontana, G., Jung, M., Schwalm, C. R., Ichii, K., Camps-Valls, G., Ráduly, B., Reichstein, M., Arain, M. A., Cescatti, A., Kiely, G., Merbold, L., Serrano-Ortiz, P., Sickert, S., Wolf, S., and Papale, D.: Predicting carbon dioxide and energy fluxes across global FLUXNET sites with regression algorithms, Biogeosciences, 13, 4291–4313, https://doi.org/10.5194/bg-13-4291-2016, 2016.

van Buuren, S.: Flexible Imputation of Missing Data, Second Edition, Chapman and Hall/CRC, Boca Raton, 2 edition edn., 2018.

Virtanen, P., Gommers, R., Oliphant, T. E., Haberland, M., Reddy, T., Cournapeau, D., Burovski, E., Peterson, P., Weckesser, W., Bright, J., van der Walt, S. J., Brett, M., Wilson, J., Millman, K. J., Mayorov, N., Nelson, A. R. J., Jones, E., Kern, R., Larson, E., Carey, C. J., Polat, I., Feng, Y., Moore, E. W., VanderPlas, J., Laxalde, D., Perktold, J., Cimrman, R., Henriksen, I., Quintero, E. A., Harris, C. R., Archibald, A. M., Ribeiro, A. H., Pedregosa, F., van Mulbregt, P., and SciPy 1.0 Contributors: SciPy 1.0: Fundamental Algorithms for Scientific Computing in Python, Nature Methods, 17, 261–272, https://doi.org/10.1038/s41592-019-0686-2, 2020.

Vogel, M. M., Orth, R., Cheruy, F., Hagemann, S., Lorenz, R., Hurk, B. J. J. M., and Seneviratne, S. I.: Regional amplification of projected changes in extreme temperatures strongly controlled by soil moisture-temperature feedbacks, Geophysical Research Letters, 44, 1511–1519, https://doi.org/10.1002/2016GL071235, https://onlinelibrary.wiley.com/doi/abs/10.1002/2016GL071235, 2017.

von Buttlar, J., Zscheischler, J., and Mahecha, M. D.: An extended approach for spatiotemporal gapfilling: dealing with large and systematic gaps in geoscientific datasets, Nonlinear Processes in Geophysics, 21, 203–215, https://doi.org/10.5194/npg-21-203-2014, 2014.

Wan, Z., Hook, S., and Hulley, G.: MYD11C1 MODIS/Aqua Land Surface Temperature/Emissivity Daily L3 Global 0.05Deg CMG V006, https://doi.org/10.5067/MODIS/MYD11C1.006, type: dataset, 2015.

Wang, Y. and Chaib-draa, B.: An online Bayesian filtering framework for Gaussian process regression: Application to global surface temperature analysis, Expert Systems with Applications, 67, 285–295, https://doi.org/10.1016/j.eswa.2016.09.018, https://linkinghub.elsevier.com/retrieve/pii/S095741741630495X, 2017.

Wehrli, K., Guillod, B. P., Hauser, M., Leclair, M., and Seneviratne, S.: Identifying Key Driving Processes of Major Recent Heat Waves, Journal of Geophysical Research: Atmospheres, 124, 11 746–11 765, https://doi.org/10.1029/2019JD030635, https://onlinelibrary.wiley.com/doi/abs/10.1029/2019JD030635, 2019.

Zeng, C., Shen, H., Zhong, M., Zhang, L., and Wu, P.: Reconstructing MODIS LST Based on Multitemporal Classification and Robust Regression, IEEE Geoscience and Remote Sensing Letters, 12, 512–516, https://doi.org/10.1109/LGRS.2014.2348651, 2015.

Zhan, X., Zheng, W., Fang, L., Liu, J., Hain, C., Yin, J., and Ek, M.: A preliminary assessment of the impact of SMAP Soil Moisture on numerical weather Forecasts from GFS and NUWRF models, 2016 IEEE International Geoscience and Remote Sensing Symposium (IGARSS), p. 4, https://doi.org/10.1109/IGARSS.2016.7730362, 2016.

Zhang, L., Liu, Y., Ren, L., Teuling, A. J., Zhang, X., Jiang, S., Yang, X., Wei, L., Zhong, F., and Zheng, L.: Reconstruction of ESA CCI satellite-derived soil moisture using an artificial neural network technology, Science of The Total Environment, 782, 146 602, https://doi.org/10.1016/j.scitotenv.2021.146602, https://linkinghub.elsevier.com/retrieve/pii/S0048969721016703, 2021.

Zhang, Q., Yuan, Q., Zeng, C., Li, X., and Wei, Y.: Missing Data Reconstruction in Remote Sensing Image With a Unified Spatial-Temporal-Spectral Deep Convolutional Neural Network, IEEE Transactions on Geoscience and Remote Sensing, 56, 4274–4288, https://doi.org/10.1109/TGRS.2018.2810208, 2018.